



## A physics-based approach to modeling real-fuel combustion chemistry – II. Reaction kinetic models of jet and rocket fuels



Rui Xu<sup>a</sup>, Kun Wang<sup>a</sup>, Sayak Banerjee<sup>a</sup>, Jiankun Shao<sup>a</sup>, Tom Parise<sup>a</sup>, Yangye Zhu<sup>a</sup>, Shengkai Wang<sup>a</sup>, Ashkan Movaghfar<sup>b</sup>, Dong Joon Lee<sup>b</sup>, Runhua Zhao<sup>b</sup>, Xu Han<sup>c</sup>, Yang Gao<sup>d</sup>, Tianfeng Lu<sup>d</sup>, Kenneth Brezinsky<sup>c</sup>, Fokion N. Egolfopoulos<sup>b</sup>, David F. Davidson<sup>a</sup>, Ronald K. Hanson<sup>a</sup>, Craig T. Bowman<sup>a</sup>, Hai Wang<sup>a,\*</sup>

<sup>a</sup> Department of Mechanical Engineering, Stanford University, Stanford, CA 94305-3032, USA

<sup>b</sup> Department of Aerospace and Mechanical Engineering, University of Southern California, Los Angeles, CA 90089-1453, USA

<sup>c</sup> Department of Mechanical and Industrial Engineering, University of Illinois at Chicago, Chicago, IL 60607, USA

<sup>d</sup> Department of Mechanical Engineering, University of Connecticut, Storrs, CT 06269-3139, USA

### ARTICLE INFO

#### Article history:

Received 21 November 2017

Revised 22 December 2017

Accepted 19 March 2018

Available online 10 April 2018

#### Keywords:

Kinetics

Jet fuel

Rocket fuel

Reaction model

HyChem

### ABSTRACT

We propose and test an alternative approach to modeling high-temperature combustion chemistry of multicomponent real fuels. The hybrid chemistry (HyChem) approach decouples fuel pyrolysis from the oxidation of fuel pyrolysis products. The pyrolysis (or oxidative pyrolysis) process is modeled by seven lumped reaction steps in which the stoichiometric and reaction rate coefficients are derived from experiments. The oxidation process is described by detailed chemistry of foundational hydrocarbon fuels. We present results obtained for three conventional jet fuels and two rocket fuels as examples. Modeling results demonstrate that HyChem models are capable of predicting a wide range of combustion properties, including ignition delay times, laminar flame speeds, and non-premixed flame extinction strain rates of all five fuels. Sensitivity analysis shows that for conventional, petroleum-derived real fuels, the uncertainties in the experimental measurements of C<sub>2</sub>H<sub>4</sub> and CH<sub>4</sub> impact model predictions to an extent, but the largest influence of the model predictability stems from the uncertainties of the foundational fuel chemistry model used (USC Mech II). In addition, we introduce an approach in the realm of the HyChem approach to address the need to predict the negative-temperature coefficient (NTC) behaviors of jet fuels, in which the CH<sub>2</sub>O speciation history is proposed to be a viable NTC-activity marker for model development. Finally, the paper shows that the HyChem model can be reduced to about 30 species in size to enable turbulent combustion modeling of real fuels with a testable chemistry model.

© 2018 The Combustion Institute. Published by Elsevier Inc. All rights reserved.

### 1. Introduction

Conventional aviation and rocket fuels are complex hydrocarbon mixtures containing hundreds to thousands of chemical compounds. Historically, combustion chemistry modeling of these fuels has taken a fuel surrogate approach [1–10]. A surrogate fuel mixture usually consists of about a half dozen of neat components, each of which may represent a certain class of the organic compounds found in the fuel. Together, the surrogate aims to reproduce the combustion chemistry behavior of a real fuel it tries to mimic. The surrogate approach simplifies the problem to an extent. It transforms a chemically intractable problem into one that can be treated by a functional reaction mechanism and

kinetics at least in theory. Practically, the surrogate approach has some drawbacks as discussed in the companion paper [11]. In the same paper, we outlined key physical evidence that supports an alternative approach to real-fuel combustion chemistry modeling. We introduced the HyChem (Hybrid Chemistry) approach and illustrated this approach to modeling the high-temperature combustion chemistry of a conventional Jet A fuel. Key findings of that study may be summarized in several key points as follows:

- (1) high-temperature combustion of large hydrocarbon fuels effectively occurs in two separate stages—fuel pyrolysis (or oxidative pyrolysis) first, followed by the oxidation of the pyrolysis products;
- (2) the oxidation of the pyrolysis products is rate limiting, and as such the accuracy of the foundational fuel chemistry model for the combustion of small species (e.g., H<sub>2</sub>, CO, CH<sub>4</sub>,

\* Corresponding author.

E-mail address: [haiwang@stanford.edu](mailto:haiwang@stanford.edu) (H. Wang).

- and C<sub>2</sub>H<sub>4</sub>) is the most critical to predicting the combustion behaviors of large hydrocarbon fuels;
- (3) it follows that the pyrolysis product distribution determines the global combustion properties of the fuel;
  - (4) for conventional petroleum-derived real fuels, key pyrolysis products are few and comprised of ethylene (C<sub>2</sub>H<sub>4</sub>), hydrogen (H<sub>2</sub>), methane (CH<sub>4</sub>), propene (C<sub>3</sub>H<sub>6</sub>), 1-butene (1-C<sub>4</sub>H<sub>8</sub>), iso-butene (*i*-C<sub>4</sub>H<sub>8</sub>), benzene (C<sub>6</sub>H<sub>6</sub>) and toluene (C<sub>7</sub>H<sub>8</sub>);
  - (5) most or all of the above species can now be measured reliably in shock tubes and flow reactors, and as such it has become feasible to employ a more direct, experimentally-based approach to describing the production rates and pyrolysis product distributions over the range of conditions critical to predicting essential combustion properties, thereby enabling the HyChem approach;
  - (6) the relevant, kinetically-controlled range of temperature of oxidative pyrolysis is around 1000 to 1450 K for most of the combustion problems; and the temperature range is comfortably accessible by the shock tube technique, and to an extent, in flow reactors;
  - (7) the HyChem approach is thus formulated, combining a set of experimentally constrained, lumped reaction steps for fuel oxidative pyrolysis with a detailed foundational fuel chemistry model to describe the pyrolysis and oxidation of the fuel pyrolysis products;
  - (8) over the temperature range just discussed, the pyrolysis product distribution, or more importantly, the stoichiometric coefficients of the lumped, fuel oxidative pyrolysis reactions should not be a function of pressure and fuel concentrations, and are only weak functions of temperature, to an extent that they can be approximated as constants;

In the current work, we present the HyChem approach and its application at a detailed level. The entire suite of methodologies and model development process is presented, from the experimental studies, the process of model development, to sensitivity analyses. The approach is applied to three jet fuels and two rocket fuels to demonstrate that HyChem models can capture the combustion behavior of a wide range of fuels. We discuss the feasibility of a HyChem-like approach to modeling the negative temperature coefficient (NTC) and low-temperature chemistry regimes of real-fuel combustion. Finally, model reduction is performed to show that about 30 species are needed to describe the high-temperature combustion chemistry of the fuels studied.

## 2. Experimental methods

### 2.1. Stanford shock tube facilities

Pyrolysis speciation and ignition delay time ( $\tau_{\text{ign}}$ ) experiments are performed using both high- and low-pressure shock tubes. Descriptions of these two facilities are provided in a recent study [12]. In brief, the high-pressure shock tube is 5.0 cm in inner diameter and uses scribed aluminum diaphragms. The low-pressure shock tube is 14.1 cm in inner diameter, and uses polycarbonate diaphragms.

Three diagnostic methods were used: pyrolysis speciation measurements via laser absorption, and  $\tau_{\text{ign}}$  measurements via OH\* emission and sidewall pressure. Laser absorption measurements took advantage of the Beer-Lambert law, i.e.  $-\ln[(I/I_0)_\lambda] = \sigma_\lambda NL$ , to relate the measured absorbance  $-\ln[(I/I_0)_\lambda]$ , with  $N$  the absorber number density and  $L$  the optical path length, to the unknown species mole fraction  $X$ , using measured absorption cross sections  $\sigma_\lambda$ . In the C<sub>2</sub>H<sub>4</sub> and CH<sub>4</sub> time-history measurements, where one product dominated the absorbance at a particular

wavelength and other species have nearly constant absorbance at this wavelength, a simple two-wavelength differential method was used to determine the concentration of the dominant absorber [13], though more quantitative methods utilizing additional wavelengths can be applied when needed.

Experimentally determined  $\tau_{\text{ign}}$  values in this study are defined as the time interval from the passage of the reflected shock wave across the observation port to the time of the measured onset of pressure rise or OH\* emission. This onset is determined by back-extrapolating the rapidly rising pressure or emission signal to the intersection with the pre-rise baseline value. For the experiments reported herein, the pressure and OH\* measurements yield results that are well within their respective experimental uncertainties.

### 2.2. UIC shock tube facilities

Pyrolysis experiments are also performed using the low-pressure single pulse shock tube (LPST) at the University of Illinois at Chicago (UIC). A detailed description of the LPST design and experimental procedure are found in earlier publications [14,15]. Briefly, the stainless-steel shock tube consists of a 1.219 m long driver section with a 10.16 cm inner bore, a 4.42 m long driven section with 6.35 cm inner bore, and a 2.54 cm thick double diaphragm buffer section that separates the other two sections. A dump tank is located in the driven section just in front of the buffer section. The shock tube operates at pressures ranging from sub-atmospheric pressure to 13 atm, at temperature between 800 K and 2000 K, and with nominal reaction time between 1 ms and 3 ms. The whole shock tube, including the dump tank, is heated at 100 °C.

The shock tube has 6 PCB 113A21 piezoelectric pressure transducers mounted in the side wall and another one mounted in the end wall. The velocity of an incident shock is calculated from the incident shock arrival times obtained from the pressure transducers in the side wall. Assuming incident shock velocity drops linearly along the distance, a relation between arrival time and distance is fitted to the measured values from the 6 pressure transducers. The velocity at the end wall is then obtained. The temperature of the reflected shock is based on the relation between the incident shock velocity and the reflected shock wave of an ideal normal shock wave using Stanford's FROSH code for concentrated, i.e. non dilute, reaction mixtures. The 2 $\sigma$  uncertainty of temperature is also calculated from the fitting of time and distance relation. The uncertainties are estimated to be between  $\pm 6$  K and  $\pm 26$  K, as will be shown later in the article. The reaction time is measured at the end wall, being the time from the shock arrival until the pressure drops to 80% of the maximum pressure [15].

The gas is sampled from the end wall after reaction quenching and transferred to a gas chromatography (GC), where the species are measured with an FID detector. The mole fraction of the fuel is determined by the carbon dioxide formed from full oxidation of the fuel/argon mixture together with the fuel average molecular formula. The 2 $\sigma$  uncertainties of the species yield, determined through both the uncertainty of single species measurement and the uncertainty of fuel mole fraction, are typically estimated to be between  $\pm 5\%$  and  $\pm 10\%$ .

### 2.3. Flow reactor facility

A flow reactor facility is used to investigate the pyrolysis and oxidative pyrolysis kinetics of jet and rocket fuels. The detailed description of the flow reactor can be found elsewhere [16]. The flow reactor is comprised of a vertical quartz reactor tube enclosed in a pressure vessel, and the tube is connected to a converging-diverging duct. A liquid fuel was injected into a vaporizer by a syringe pump before being introduced into the reactor in a nitrogen carrier gas. The fuel vapor-nitrogen mixture

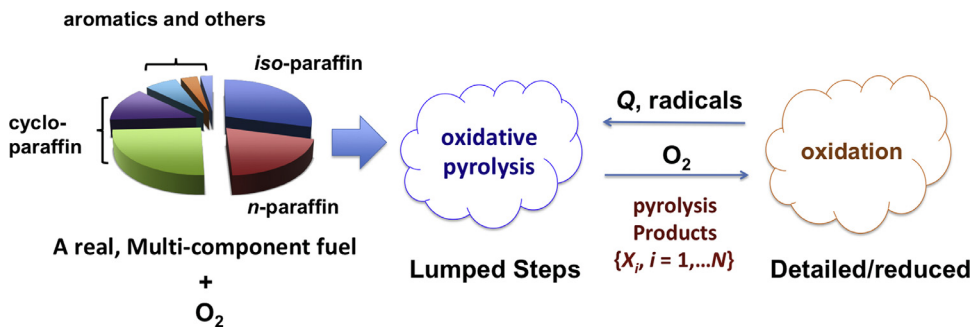


Fig. 1. Schematic of the HyChem approach.

is injected into the products of, a  $H_2$ /air flame stabilized on a water-cooled McKenna burner to provide a hot vitiated flow into the tube. To ensure that the reaction takes place under near adiabatic conditions, the quartz reactor tube is electrically heated by temperature-controlled heaters.

The reaction products are sampled by a cooled extraction probe and are sent to a 4-column micro gas chromatograph (Inficon microGC 3000) that provides real-time detection. A non-dispersive infrared analyzer (NDIR) and a paramagnetic analyzer (PMA) were used for real-time measurements of  $CO$ ,  $CO_2$  and  $O_2$  for comparison with the GC measurements. The total uncertainty in species concentration is  $\pm 2$  to  $\pm 5\%$  for most species.

#### 2.4. Laminar flame speeds and extinction strain rates

Laminar flame speed,  $S_u^\circ$ , is measured in the counterflow configuration for a wide range of equivalence ratios at atmospheric pressure and an unburned mixture temperature  $T_u = 403$  K. The liquid fuel system consists of a high-pressure precision pump that supplies fuel into a quartz nebulizer and is sprayed into preheated stream of air. A double pulsed ND:YAG laser and a high performance 12 bit CCD camera with  $1376 \times 1040$  pixels of resolution were used to acquire Particle Image Velocimetry (PIV) images. The minimum axial velocity along the system centerline just upstream of the flame is defined as a reference flame speed,  $S_{u,\text{ref}}$ , and the maximum absolute value of axial velocity gradient is defined as a local strain rate,  $K$ . As  $K$  is varied, its effect on  $S_{u,\text{ref}}$  is recorded, and  $S_u^\circ$  is determined through computationally-assisted extrapolation to zero stretch [17]. The  $2\sigma$  standard deviations in  $S_u^\circ$  are indicated with uncertainty bars in relevant figures.

Extinction strain rates,  $K_{\text{ext}}$ , are measured also in the counterflow configuration at atmospheric pressure for non-premixed flames by impinging a fuel/ $N_2$  stream at  $T_u = 473$  K onto an ambient temperature  $O_2$  stream. In order to determine the  $K_{\text{ext}}$ , a near-extinction flame is established, and then the strain rate  $K$  is measured on the fuel side and extinction is achieved by reducing slightly the fuel concentration.

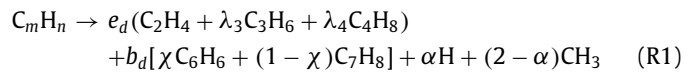
High-pressure  $S_u^\circ$ 's were measured in the constant volume spherical expanding flame configuration. Details of the spherical chamber can be found elsewhere [18]. The chamber, with an internal diameter of 203.2 mm, is made of stainless steel and can withstand post-combustion pressure up to 200 atm. The chamber has no optical access, so the only observable is the pressure time history. The flame speed can be further determined using the direct numerical method and hybrid thermodynamic-radiation model. Details of the derivation procedure are reported separately [18].

#### 3. HyChem model formulation

As discussed earlier [11], the HyChem model expresses fuel pyrolysis and oxidation of the pyrolysis products in two separate

submodels. Figure 1 shows a schematic of the structure of a HyChem model. The oxidative pyrolysis of the fuel is modeled by several experimentally constrained, lumped reaction steps. The rate of the oxidation of the pyrolysis products is critical to radical growth and heat release, and for this reason it is modeled with a detailed foundational chemistry model for oxidation of the pyrolysis products. USC Mech II [19] is used here for this purpose. As shown in Fig. 1, the two submodels are interconnected: the pyrolysis process provide the "reactants" for the oxidation process, while the oxidation process supplies heat and radical species to facilitate the endothermic, oxidative pyrolysis of the fuel.

Key assumptions of the HyChem approach have been discussed earlier [11]. A small number of pyrolysis intermediates are produced from the multicomponent fuel mixture first during its combustion. From flow reactor measurements (to be discussed later), the following species are found to be the key pyrolysis products:  $C_2H_4$ ,  $C_3H_6$ ,  $i-C_4H_8$ ,  $C_6H_6$ ,  $C_7H_8$ , and  $H_2$ . For a fuel with an average molecular formula of  $C_mH_n$ , the reactions are cast into the following reaction equations:



where

$$\Sigma_p = \gamma CH_4 + e_a(C_2H_4 + \lambda_3C_3H_6 + \lambda_4C_4H_8) + b_a[\chi C_6H_6 + (1 - \chi)C_7H_8] + \beta H + (1 - \beta)CH_3.$$

In the above formulation,  $\lambda_3$  represents the ratio of  $C_3H_6$ -to- $C_2H_4$ ,  $\lambda_4$  is the ratio of  $C_4H_8$ -to- $C_2H_4$ ,  $\chi$  is the ratio of  $C_6H_6$  to the sum of  $C_6H_6$  and  $C_7H_8$ ,  $\gamma$  accounts for the yield of  $CH_4$  in addition to its production from H-abstraction by the  $CH_3$  radical, and  $\alpha$  and  $\beta$  are the branching ratios of the H atom to the  $CH_3$  radicals from reactions R1 and R2–7, respectively. We note that the first reaction step yields two radicals and the second conserves the number of radicals as one would expect for these types of the reactions. The exact nature of the radical products assigned in

**Table 1**  
Independent, stoichiometric parameters.

Parameter	Descriptions	Range	Method of determination
$\alpha$	number of H atoms produced in the “C–C fission reaction” (R1) per $C_mH_n$	[0, 2]	Shock-tube time history ( $C_2H_4$ and $CH_4$ )
$\beta$	number of H atoms produced in the H-abstraction reactions (R2–7) per $C_mH_n$	[0, 1]	Shock-tube time history ( $C_2H_4$ and $CH_4$ )
$\gamma$	$CH_4$ yield per $C_mH_n$ in addition to H abstraction by $CH_3$ .	[0, $\gamma_{max}$ ] <sup>a</sup>	Shock-tube time history ( $C_2H_4$ and $CH_4$ )
$\lambda_3$	$[C_3H_6]/[C_2H_4]$	[0, $\infty$ ]	Flow-reactor speciation
$\lambda_4$ <sup>b</sup>	$[C_4H_8]/[C_2H_4]$	[0, $\infty$ ]	Flow-reactor speciation
$\chi$	$[C_6H_6]/([C_6H_6] + [C_6H_5CH_3])$	[0, 1]	Flow-reactor speciation

<sup>a</sup>  $\gamma_{max} = [-(4 - \chi)m + \frac{1}{2}(7 - \chi) + 3\beta]/(10 - \chi) - 1$ .

<sup>b</sup>  $\lambda_4 = \lambda_{4,1} + \lambda_{4,i}$ .

reaction (R1) is not as important. This may be evidenced by the minuscule sensitivity of prediction results of model predictions to the  $\alpha$  parameter. In principle,  $\gamma$  can be set to zero, but we nonetheless retain the  $\gamma$  parameter for generality. For real fuels,  $m$  and  $n$  can be of non-integer, but considering that a majority of computer codes can only handle integer molecular formula, we treat  $m$  and  $n$  as integers here. Additionally, the  $C_4H_8$  expressed in the above reactions is the sum of 1- $C_4H_8$  and  $i$ - $C_4H_8$ . For this reason,  $\lambda_4 = \lambda_{4,1} + \lambda_{4,i}$ , where  $\lambda_{4,1}$  and  $\lambda_{4,i}$  are related to the yield of 1- $C_4H_8$  and  $i$ - $C_4H_8$ , respectively.

Reaction (R1) represents the initial radical production through the C–C fission in the fuel “molecule”. The radicals produced are H and  $CH_3$ , which can further attack the fuel “molecule” as described in reactions (R2–7). In principle, the H-abstraction reaction produces the fuel radical first in the rate-limiting step of fuel disappearance, and as such the H-abstraction and the subsequent  $\beta$ -scission of the fuel radical are combined into a single step.

A key constraint in the stoichiometric coefficients expressed in reactions (R1–7) is the elemental conservation. The balances of the C and H elements require that

$$m = e_d(2 + 3\lambda_3 + 4\lambda_4) + b_d(7 - \chi) - \alpha + 2 \quad (1)$$

$$\frac{n}{2} = e_d(2 + 3\lambda_3 + 4\lambda_4) + b_d(4 - \chi) - \alpha + 3 \quad (2)$$

$$m = e_a(2 + 3\lambda_3 + 4\lambda_4) + b_a(7 - \chi) + \gamma - \beta + 1 \quad (3)$$

$$\frac{n}{2} = e_a(2 + 3\lambda_3 + 4\lambda_4) + b_a(4 - \chi) + 2\gamma - \beta + 2 \quad (4)$$

Manipulation of the above equations yields the expressions of the dependent stoichiometric parameters as

$$e_d = \frac{[-(4 - \chi)m + \frac{(7 - \chi)}{2}n + 3\alpha + \chi - 13]}{3(2 + 3\lambda_3 + 4\lambda_4)} \quad (5)$$

$$e_a = \frac{[-(4 - \chi)m + \frac{(7 - \chi)}{2}n + 3\beta - (10 - \chi)\gamma - (10 - \chi)]}{3(2 + 3\lambda_3 + 4\lambda_4)} \quad (6)$$

$$b_d = \frac{1}{3}\left(m - \frac{n}{2} + 1\right) \quad (7)$$

$$b_a = \frac{1}{3}\left(m - \frac{n}{2} + \gamma + 1\right) \quad (8)$$

Hence, there are a total of seven independent stoichiometric parameters,  $\alpha$ ,  $\beta$ ,  $\gamma$ ,  $\lambda_3$ ,  $\lambda_{4,1}$ ,  $\lambda_{4,i}$  and  $\chi$ . Table 1 presents the physical description, bounds, and the methods of determination for these parameters. Three parameters ( $\lambda_3$ ,  $\lambda_4$  and  $\chi$ ) can be estimated directly from the flow reactor experiments and then are adjusted through measured species time histories from flow reactor and shock tube under a prescribed range of conditions along with the other three variables  $\alpha$ ,  $\beta$ , and  $\gamma$ . The values of  $\alpha$  and  $\beta$  are related to the production of two key species, namely

the H atom and  $C_2H_4$  for the fuels studied here. They directly impact the fuel disappearance rate.

Assuming that all the stable decomposition products are produced from the H-abstraction reactions without the complication of secondary reactions, the yields for the pyrolysis products can be calculated as follows:

$$y_{CH_4,\infty} \approx 1 - \beta + \gamma \quad (12)$$

$$y_{C_2H_4,\infty} \approx e_a \quad (13)$$

$$= \frac{1}{3} \frac{[-(4 - \chi)m + \frac{1}{2}(7 - \chi)n - (10 - \chi)\gamma + 3\beta - (10 - \chi)]}{2 + 3\lambda_3 + 4\lambda_4}$$

$$y_{C_6H_6,\infty} \approx e_a \lambda_{4,1} \quad (14)$$

$$= \frac{1}{3} \left[ \frac{[-(4 - \chi)m + \frac{1}{2}(7 - \chi)n - (10 - \chi)\gamma + 3\beta - (10 - \chi)]}{2 + 3\lambda_3 + 4\lambda_4} \right] \lambda_{4,1}$$

$$y_{1-C_4H_8,\infty} \approx e_a \lambda_{4,1} \quad (15)$$

$$= \frac{1}{3} \left[ \frac{[-(4 - \chi)m + \frac{1}{2}(7 - \chi)n - (10 - \chi)\gamma + 3\beta - (10 - \chi)]}{2 + 3\lambda_3 + 4\lambda_4} \right] \lambda_{4,1}$$

$$y_{i-C_4H_8,\infty} \approx e_a \lambda_{4,i} \quad (15')$$

$$= \frac{1}{3} \left[ \frac{[-(4 - \chi)m + \frac{1}{2}(7 - \chi)n - (10 - \chi)\gamma + 3\beta - (10 - \chi)]}{2 + 3\lambda_3 + 4\lambda_4} \right] \lambda_{4,i}$$

$$y_{C_6H_6,\infty} = b_a \chi = \frac{1}{3} \left( m - \frac{n}{2} + \gamma + 1 \right) \chi \quad (16)$$

$$y_{C_7H_8,\infty} = b_a (1 - \chi) = \frac{1}{3} \left( m - \frac{n}{2} + \gamma + 1 \right) (1 - \chi) \quad (17)$$

Figure 2 shows the possible variations of  $CH_4$ , and  $C_6H_6$  or  $C_7H_8$  yields as a function of the  $C_2H_4$  yield over a range of  $\gamma$  values. The calculation is made by assuming the ratio of  $C_3H_6$ -to- $C_2H_4$  ( $\lambda_3$ ) and  $C_4H_8$ -to- $C_2H_4$  ( $\lambda_4$ ) to be 0.4 and 0.2, respectively and these values have been discussed in Ref. [11]. The narrow bands in the figure indicate that the elemental balances impose strong constraints on the possible yield ratios of the pyrolysis intermediates. Measurement of the  $C_2H_4$  yield under suitable conditions will give approximately the  $CH_4$  yield, and likewise a narrow range of  $C_6H_6$  or  $C_7H_8$  yield. To demonstrate the above point, representative experimental data of four different jet and rocket fuels, along with their error bars, are included in the left panel of Fig. 2. The  $C_2H_4$  and  $CH_4$  yield data shown were obtained for fuel pyrolysis at  $T_5$  around 1250 K after 2 ms reaction time in a shock tube, at which time the fuel is completely consumed. Similarly, the combined yields of benzene and toluene versus the yield of ethylene from oxidative pyrolysis of three jet fuels are plotted in the right panel of Fig. 2. Clearly, the measured values fall well within the respective yield bands due to elemental balances. The point of this

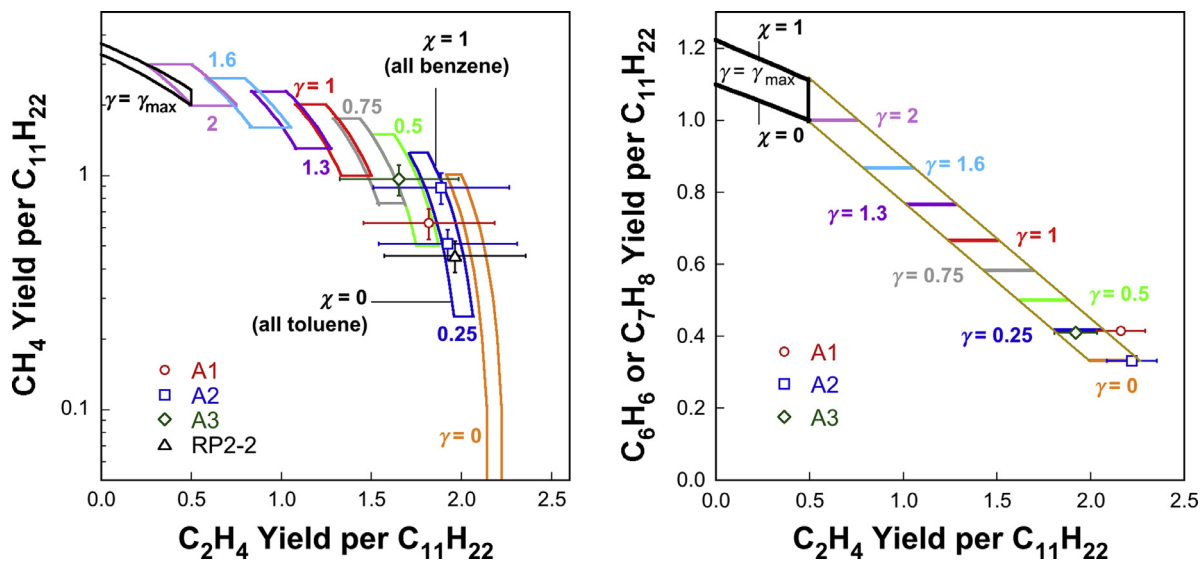


**Fig. 2.** Variations of  $\text{CH}_4$  (left panel) and  $\text{C}_6\text{H}_6$  or  $\text{C}_7\text{H}_8$  yields (right panel) as a function of the  $\text{C}_2\text{H}_4$  yield per one  $\text{C}_{11}\text{H}_{22}$  molecule over a range of  $\gamma$  values. The symbols are based on representative experimental measurements of  $\text{C}_2\text{H}_4$  and  $\text{CH}_4$  yields at 2 ms in shock tube pyrolysis of several fuels at  $p_5 = 12.4$  atm,  $T_5 \sim 1250$  K (left panel), and  $\text{C}_6\text{H}_6 + \text{C}_7\text{H}_8$  at 20 ms of reaction time for fuel oxidative pyrolysis in a flow reactor ( $p = 1$  atm,  $T = 1140$  K and 300 ppm fuel).

**Table 2**

Key properties of the fuels studied [21].

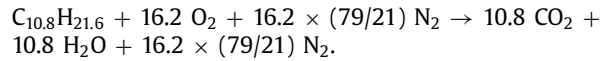
Fuel	Average Formula	H/C ratio	MW (g/mol)	LHV (MJ/kg)	Composition (Mass %)				Model Formula
					<i>n</i> -paraffin	iso-paraffin	c-paraffin	aromatics	
A1	$\text{C}_{10.8}\text{H}_{21.6}$	2.00	151.9	43.2	26.8	39.7	20.1	13.4	$\text{C}_{11}\text{H}_{22}$
A2	$\text{C}_{11.4}\text{H}_{21.7}$	1.90	158.6	43.1	20.0	29.4	31.9	18.7	$\text{C}_{11}\text{H}_{22}$
A3	$\text{C}_{12.0}\text{H}_{22.3}$	1.86	166.1	42.9	13.9	18.1	47.4	20.6	$\text{C}_{12}\text{H}_{23}$
RP2-1	$\text{C}_{12.0}\text{H}_{24.1}$	2.01	167.9	43.6	2.4	36.6	60.7	0.3	$\text{C}_{12}\text{H}_{24}$
RP2-2	$\text{C}_{12.6}\text{H}_{25.6}$	2.04	177.0	43.8	13.4	39.7	46.2	0.7	$\text{C}_{13}\text{H}_{27}$

analysis is that elemental conservation supersedes thermodynamic and chemical kinetic constraints, as expected. It follows that if the pyrolysis product distribution is the most critical to predicting the combustion behaviors of a real fuel, as we discussed in Ref. [11], only a limited number of internally correlated measurements are needed to constrain the lumped reaction model formulated above.

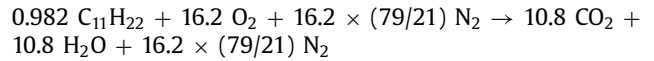
#### 4. Modeling approach

We consider three conventional, petroleum-derived jet fuels: JP-8, Jet A and JP-5, designated here as A1, A2 and A3, respectively [20], and two rocket fuels, designated here as RP2-1 and RP2-2. Key properties and compositions are listed in Table 2. It is necessary to use integer molecular formulae only because of computer code limitations. The model formulae are listed in the last column of Table 2. Except for RP2-2, the model formulae are the closest integer round-offs of the respective actual average formulae. The enthalpy of formation is determined from the lower-heating value (LHV). The entropy and specific heat are estimated by using a fuel surrogate mixture that closely matches the H/C ratio, mean molecular weight, and class composition of a given fuel. Details can be found in the Supplementary Materials. The model formula of RP2-2 ( $\text{C}_{13}\text{H}_{27}$  versus the actual  $\text{C}_{12.6}\text{H}_{25.6}$ ) is based on the considerations of both the H/C ratio and its thermochemical surrogate mixture, which is closer to  $\text{C}_{13}\text{H}_{27}$  than to  $\text{C}_{13}\text{H}_{26}$ .

The small difference in the actual and model chemical formulae causes a minor problem, in that the equivalence ratio and mass fraction of the fuel cannot be simultaneously matched. Here we propose that the fuel mass be matched in a fuel-oxidizer-diluent mixture. For example, the actual stoichiometric reaction of the A1-air mixture is



In simulations, we use instead



where the value 0.982 comes from  $\text{MW}(\text{C}_{10.8}\text{H}_{21.6})/\text{MW}(\text{C}_{11}\text{H}_{22})$ .

Kinetic modeling was carried out using the Sandia Chemkin code [22] for initial value problems. The ignition delay time in a shock tube was identified as the time to the maximum rate of  $\text{OH}^*$  production. The choice for the maximum rate differs somewhat from the experiment in which the inflection point was chosen as the ignition measure, which occurs slightly before the maximum  $\text{OH}^*$  production rate, but the constant volume assumption in modeling compensates for this effect, as the real experimental condition is between constant volume and constant pressure. The laminar flame speed was calculated using PREMIX [23] with multicomponent transport and thermal diffusion. The non-premixed flame extinction strain rate was computed using a modified opposed-jet flow code [24] developed originally by Kee et al. [25]. A two-point continuation method was used to obtain the extinction strain rates at the state of extinction [26]. The binary diffusion coefficients of the fuels are based on values reported recently [27–29], assuming that the average binary diffusion coefficient of the fuel is equal to the diffusion coefficient of a straight-chain *n*-alkane of the same carbon number in the molecule. For example, the binary diffusion coefficients of A2 in other gases are assigned the values of those of *n*-undecane ( $n\text{-C}_{11}\text{H}_{24}$ ) and those of A3 are equal to the diffusion coefficients of *n*-dodecane ( $n\text{-C}_{12}\text{H}_{26}$ ).

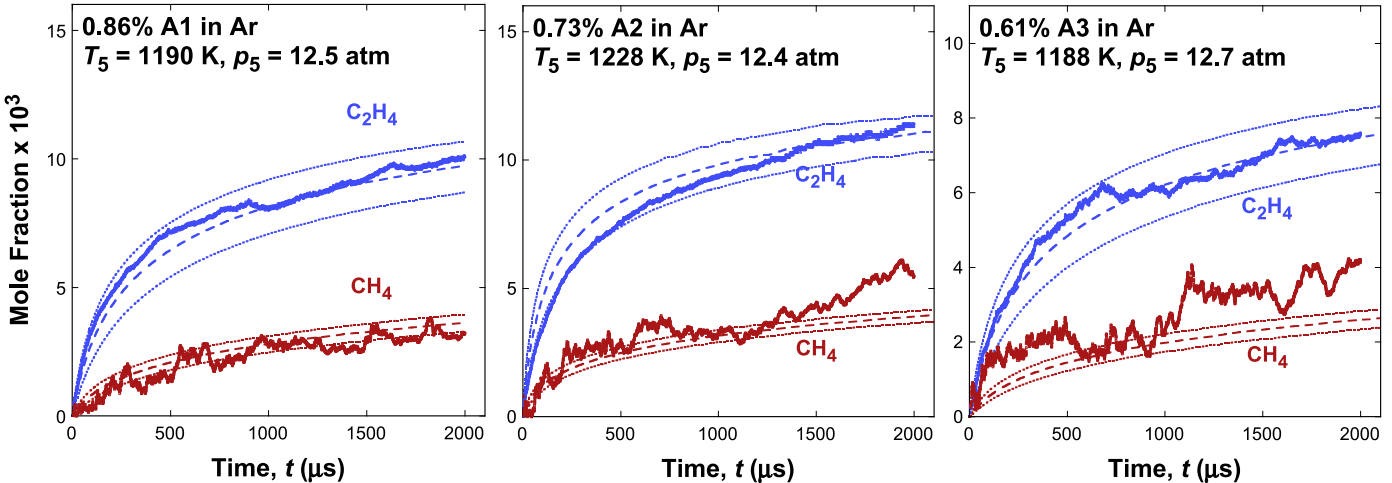


**Fig. 3.** Time histories of  $\text{C}_2\text{H}_4$  and  $\text{CH}_4$  measured (solid lines) and simulated (dashed lines) from thermal decomposition of A1 (left), A2 (middle), and A3 (right) fuel in argon in the Stanford shock tube. The dotted lines are simulations bracketing the  $\pm 15$  K temperature uncertainty.

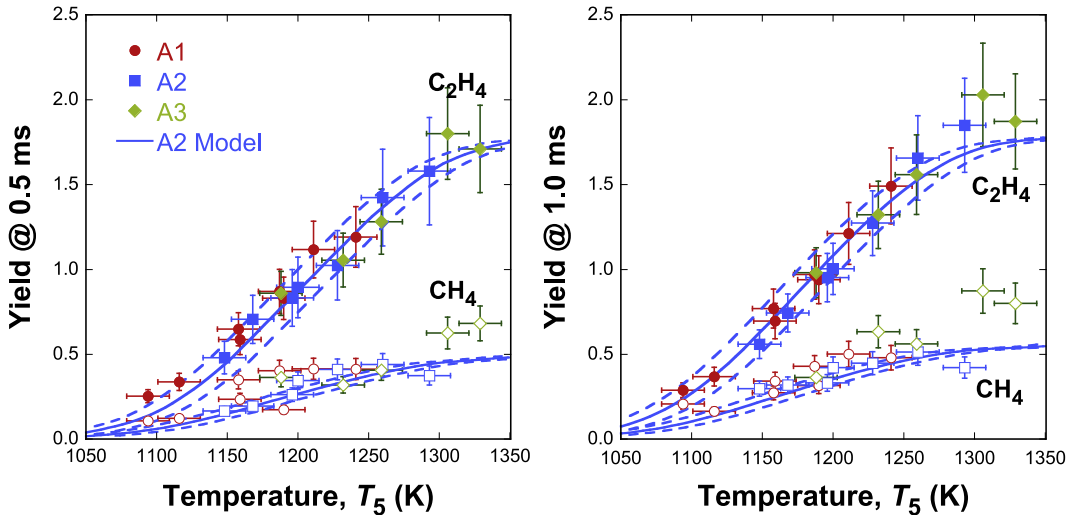


**Fig. 4.** Yields of  $\text{C}_2\text{H}_4$  and  $\text{CH}_4$  measured (symbols) and simulated (lines) from thermal decomposition of 0.73 % (mol) A1, A2, and A3 fuel in argon in the Stanford shock tube at a nominal pressure  $p_5 = 12.4$  atm. The dashed lines are simulations bracketing the  $\pm 15$  K temperature uncertainty. Error bars represent  $\pm 15$  K in temperature uncertainty and experimental uncertainties of  $\text{C}_2\text{H}_4$  and  $\text{CH}_4$  concentrations.

## 5. Results and discussion

### 5.1. Derivation of model parameters

As discussed in Ref. [11], the parameters  $\lambda_3$ ,  $\lambda_{4,1}$ ,  $\lambda_{4,i}$ , and  $\chi$  are initially estimated based on the ratios of  $[\text{C}_3\text{H}_6]/[\text{C}_2\text{H}_4]$ ,  $[\text{1-C}_4\text{H}_8]/[\text{C}_2\text{H}_4]$ ,  $[\text{i-C}_4\text{H}_8]/[\text{C}_2\text{H}_4]$  and  $[\text{C}_6\text{H}_6]/([\text{C}_6\text{H}_6] + [\text{C}_6\text{H}_5\text{CH}_3])$  measured in the flow reactor. The reaction rate coefficients  $k_i$  ( $i = 1, 2, \dots, 7$ ) are estimated initially from the analogous reactions of *n*-dodecane in JetSurF [30,31]. These model parameters, along with  $\alpha$  and  $\beta$ , are then jointly fitted to the  $\text{C}_2\text{H}_4$  and  $\text{CH}_4$  time history data from shock tube pyrolysis and oxidative pyrolysis, and flow reactor oxidative pyrolysis experiments. As examples, Fig. 3 shows the  $\text{C}_2\text{H}_4$  and  $\text{CH}_4$  time history profiles in shock tube pyrolysis of A1, A2, and A3 in argon, each at a given initial temperature. The dotted lines are simulations considering  $\pm 15$  K uncertainty in the experimental  $T_5$  value. Figure 4 shows the  $\text{C}_2\text{H}_4$  and  $\text{CH}_4$  yields at two representative reaction times, 0.5 and 1.0 ms, during shock tube pyrolysis of the three jet fuels over the temperature of 1080–1350 K. As seen, the model is capable of reconciling the yield data over a range of temperatures. Additionally, the three jet fuels tested yield nearly the same amounts of  $\text{C}_2\text{H}_4$  and  $\text{CH}_4$

under comparable conditions (and the same global combustion properties, including ignition delay and laminar flame speed, as will be discussed later). This finding is another illustration of the insensitivity of the basic combustion responses to fuel composition (including the batch to batch variations) as we explained in the companion paper [11]. That is, in a fuel mixture in which the H/C ratio falls within a certain range and the number of components is large enough, the pyrolysis product distribution and combustion properties (e.g., ignition delay time and laminar flame speed) appear to vary little.

Tests show that the time profiles of  $\text{C}_2\text{H}_4$  and  $\text{CH}_4$  pose the strongest constraints on the  $\alpha$  and  $\beta$  values, which govern the ratio of the reactive radical  $\text{H}$  to the less-reactive radical  $\text{CH}_3$ . An increase in the  $\alpha$  and  $\beta$  value would increase both the  $\text{C}_2\text{H}_4$  mole fraction and its initial rate of production, but it reduces the  $\text{CH}_4$  mole fraction. The reaction rate coefficients  $k_1$ ,  $k_2$ , and  $k_3$  impact the time history profile, but to a smaller extent than  $\alpha$  and  $\beta$ . While  $k_1$  can impact the initial production rate and final mole fractions of  $\text{C}_2\text{H}_4$  and  $\text{CH}_4$ ,  $k_2$  affects only the initial slope of the  $\text{C}_2\text{H}_4$  and  $\text{CH}_4$  time histories. An increase of  $k_3$  would increase the  $\text{CH}_4$  production noticeably.

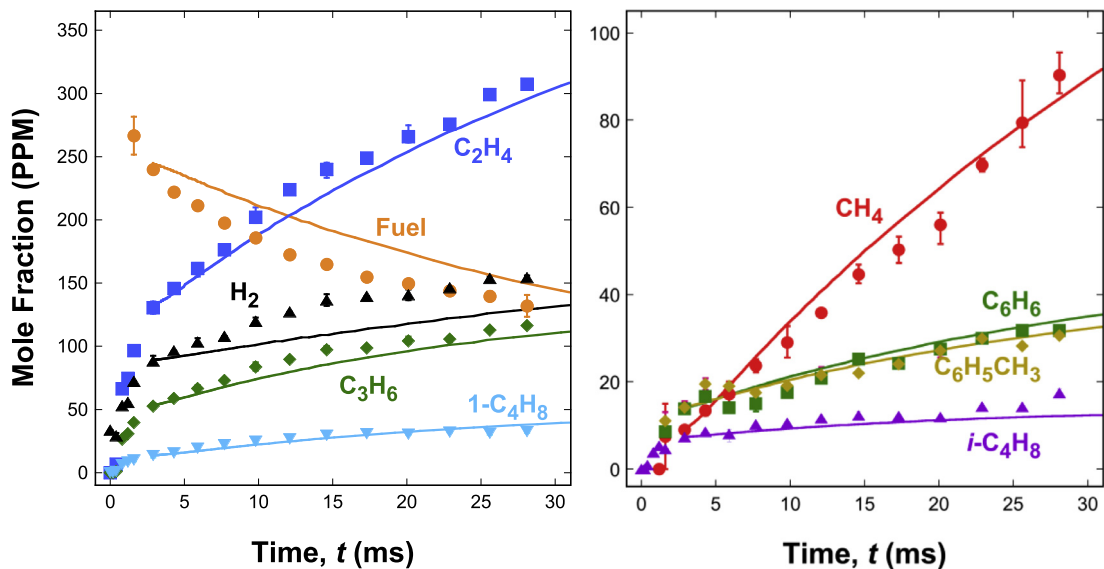


**Fig. 5.** Time histories of major oxidative pyrolysis species during the early stage of A2 oxidation (314 ppm A2 in a vitiated oxygen-nitrogen mixture at unity equivalence ratio) in a flow reactor at 1030 K temperature and 1 atm pressure. Symbols are experimental data; lines are simulations starting at 2.87 ms using measured species concentration as input of the initial condition. The concentrations of these species, including those from the vitiated mixture, are given in Table S1 of the Supplementary Materials.

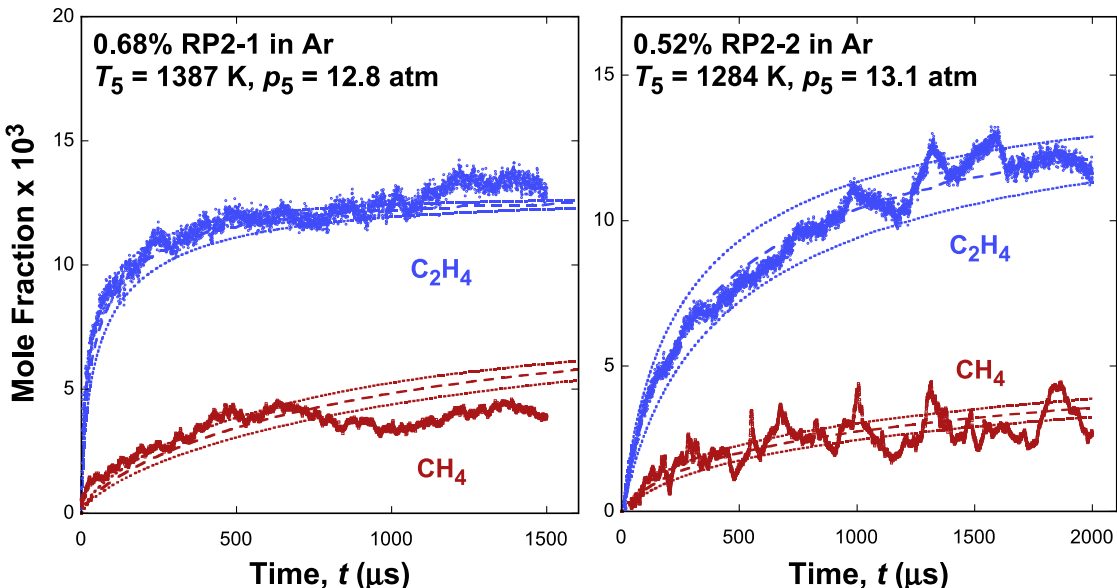


**Fig. 6.** Time histories of  $\text{C}_2\text{H}_4$  and  $\text{CH}_4$  measured and simulated (dashed line) from thermal decomposition of RP2-1 (left) and RP2-2 (right) fuel in argon in the Stanford shock tube. The dotted lines are simulations bracketing the  $\pm 15$  K temperature uncertainty.

The measured time evolution of the key species in the flow reactor during fuel oxidative pyrolysis places joint constraints on the rate coefficients and stoichiometric parameters. Figure 5 shows the result of a joint fit to the flow reactor data using the A2 data as an example. It is seen that the agreement with the data is satisfactory. Test shows that the fuel decay profile is useful for estimating  $k_4$  and  $k_5$ . It was found that  $k_6$  and  $k_7$  are difficult to determine from species data available as they are usually too slow to be of any importance in these experiments. For now,  $k_7$  is assumed to be that of *n*-dodecane. Ignition delay time at one single temperature within 1000–1100 K is consulted for  $k_6$  estimation. Work is underway to identify a suitable set of oxidative pyrolysis speciation experiment for constraining  $k_6$  and  $k_7$ .

The RP2 models are derived similarly. Figure 6 shows sample time profiles of  $\text{C}_2\text{H}_4$  and  $\text{CH}_4$  mole fraction during shock tube RP2 pyrolysis. Figure 7 presents the  $\text{C}_2\text{H}_4$  and  $\text{CH}_4$  yields at fixed

reaction time of 0.5 and 1.0 ms over a range of  $T_5$  and a nominal  $p_5$  of 13.5 atm. The  $\text{C}_2\text{H}_4$  yields differ somewhat between the two RP2 fuels. The cause is probably in the significant difference of the *n*-paraffin concentrations in the fuel: while RP2-2 contains about 13 % *n*-paraffins, RP2-1 contains only ~2 % *n*-paraffins.

Species time histories from oxidative pyrolysis experiments are also useful as these experiments provide some constraints to  $k_4$ ,  $k_5$ ,  $k_6$ , and  $k_7$ . Figure 8 shows the  $\text{C}_2\text{H}_4$  yields from A2 pyrolysis and oxidative pyrolysis at unity equivalence ratio in the Stanford shock tube facility under a normal pressure of 1.6 atm. Overall, the model results are in close agreement with the experimental data.

## 5.2. Testing the models

The HyChem models are available in the Supplementary Materials along with their thermochemical data and transport database.

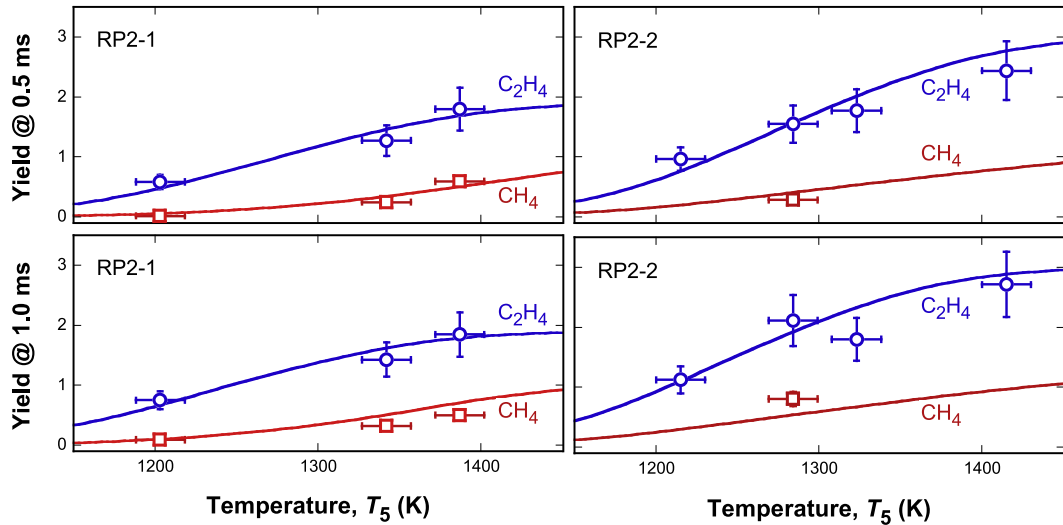


**Fig. 7.** Yields of  $\text{C}_2\text{H}_4$  and  $\text{CH}_4$  measured (symbols) and simulated (lines) from thermal decomposition of 0.76 % (mol) RP2-1 and RP2-2 in Ar in the Stanford shock tube at  $p_5 = 13.5$  atm.

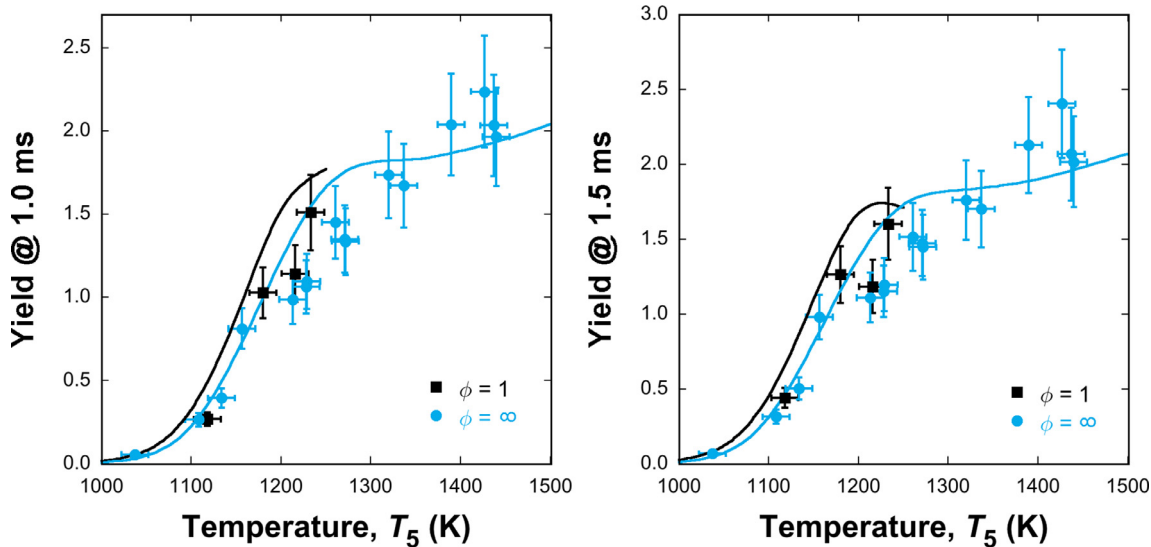


**Fig. 8.** Yields of  $\text{C}_2\text{H}_4$  measured (symbols) and simulated (lines) from the oxidation ( $\phi = 1$ ) and pyrolysis, both at 0.4 % (mol) A2 with argon as the balance gas in the Stanford shock tube at  $p_5 = 1.6$  atm. Error bars represent  $\pm 15$  K in temperature uncertainty and experimental uncertainties of  $\text{C}_2\text{H}_4$  and  $\text{CH}_4$  concentrations.

The models are tested against a wide range of experiments, including the pyrolysis species yields from the UIC single-pulse shock tube facility, ignition delay time, laminar flame speed and non-premixed flame extinction strain rates under atmospheric pressure, and laminar flame speed at elevated pressures. Additional literature data are available for jet fuels, including shock tube ignition delay [32–36], laminar flame speed [37–40], counterflow laminar flame extinction and/or ignition [39,41–45]. Comparisons of the HyChem model predictions against the counterflow flame extinction and ignition data of Seshadri and coworkers [43] are presented and discussed in the Supplementary Materials.

Figure 9 shows the yields of relevant species during 0.63% (mol) A2 pyrolysis in argon at a nominal pressure of 12.4 atm in the single-pulse shock tube at UIC. The dwell time ranges from 1.85 to 2.39 ms. Simulations are carried out under the condition of each specific shock run. It is seen that the model captures the yields of key species generally well, including  $\text{C}_2\text{H}_4$ ,  $\text{CH}_4$ ,  $\text{C}_3\text{H}_6$ ,  $1\text{-C}_4\text{H}_8$  and  $i\text{-C}_4\text{H}_8$ . Minor discrepancies are observed for the species concentrations measured in the Stanford and UIC shock tube facilities. These discrepancies should not impact the model

accuracy to an appreciable extent especially when they are used for flame and ignition delay predictions, as will be discussed later.

The HyChem models reproduce the ignition delay times of the five fuels well over a range of temperatures, pressures, equivalence ratios, and the type of diluent (Ar versus  $\text{N}_2$ ) as shown in Fig. 10. It is seen that overall, the simulated ignition delay times are in good agreement with their respective experimental counterparts. In particular, the ignition delay data of A1 and A2 span a pressure range substantially wider than that of the speciation data from shock tube (12–15 atm) and flow reactor (1 atm) from which the parameters of the fuel pyrolytic submodel were derived. We do not see progressive worsening of the predictive quality of the model towards high pressures. This indicates the extrapolative capability of the HyChem model and thus supports the validity of its approach to an extent. The figures for A1, A2 and A3 also include the predictions by their respective NTC-enabled HyChem model (dashed lines) for selected mixtures. While the details about the NTC submodel will be introduced later, we note that NTC chemistry is likely to impact the low-temperature, high-pressure data shown in Fig. 10.

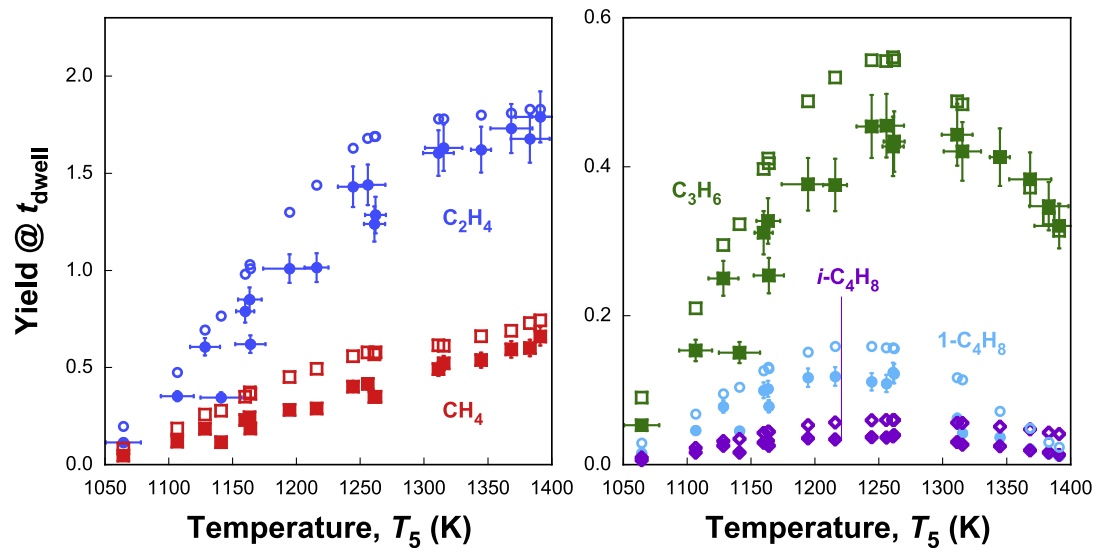


**Fig. 9.** Measured (closed symbols) and simulated (open symbols) species yields from thermal decomposition of 0.63% A2 in argon at a nominal pressure of  $p_5 = 12.4$  atm in the UIC single-pulse shock tube. The dwell time ranges from 1.85 to 2.39 ms. Error bars represent temperature uncertainty determined from shock velocity and experimental uncertainties of the species concentrations.

Likewise, the models reproduce the laminar flame speeds of the fuels considered over an extended range of equivalence ratios at atmospheric pressure and 403 K unburned gas temperature (Fig. 11 left panel) and elevated pressures (Fig. 12) for two equivalence ratios (0.9 and 1.05) rather well. In general, the model predictions lie within  $\pm 2\sigma$  uncertainties of the data. A slight underprediction of the experimental data is observed for the high-pressure flames. It is possible that the discrepancies stem from our insufficient knowledge about the Chaperon efficiency of He, yet other causes are also equally possible. Simulations using experimental pressure time history during compression show that fuel decomposition and oxidation to be unimportant below 15 atm. Figure 13 shows a typical ranked sensitivity spectrum computed for A2 under a representative condition of the experiment, i.e., 10.6 atm unburned gas pressure and 0.9 equivalence ratio. Clearly, the most important reactions are chain branching and chain termination reactions; fuel-related lumped reactions do not play a notable role in the flame speed prediction under the conditions shown in Fig. 12. If the discrepancies are attributable to the Chaperon efficiency of He, the effects should be exhibited in the  $\text{H} + \text{O}_2 (+\text{M}) = \text{HO}_2 (+\text{M})$  and  $\text{H} + \text{CH}_3 (+\text{M}) = \text{CH}_4 (+\text{M})$  reactions, as they are ranked third and fourth on the ranked sensitivity spectrum, as seen in Fig. 13.

Figure 11 also shows the experimental and model comparisons for  $K_{\text{ext}}$  of non-premixed fuel/ $\text{N}_2$  jet against  $\text{O}_2$ . As discussed in the companion paper [11], the extinction strain rate of a non-premixed flame is sensitive to the diffusion coefficient of the fuel. When a range of jet/rocket fuels were examined, we found it to be adequate to model the binary diffusion coefficients of the real “fuel” of an average molecular formula of  $\text{C}_m\text{H}_n$  by those of a  $\text{C}_{11}\text{H}_{22}$  *n*-alkane. The latter were taken from results in a series of recent work on the diffusion coefficients of long-chain molecules and dependence of the counter-flow flame extinction on the molecular diffusivity of large fuels [27–29]. As Fig. 11 shows, this approximation provides a good prediction for  $K_{\text{ext}}$ . Since the  $m$  value of the five fuel considered spans from 11 to 13, we plot in panel (b) (the A2 fuel) of Fig. 11 the predictions made for  $m = 10$  and 12 for an otherwise “ $\text{C}_{11}\text{H}_{22}$ ” fuel. As seen, the sensitivity is apparent but not strong. The comparison shown should thus be viewed as an important test about the ability of the model to reproduce the extinction strain rate data.

In so far as the global combustion properties are concerned, the three jet fuels tested exhibit nearly the same chemical behaviors

and global combustion properties. The only notable difference stems from the mean molecular weight of the three fuels. The A3 fuel has a slightly higher molecular weight and the effect is captured by the somewhat smaller extinction strain rate ( $\sim 10\%$ ) than the other two fuels.

### 5.3. Sensitivity with respect to measured species concentration

The HyChem model parameters are determined by matching species time histories in the fuel pyrolysis and oxidative pyrolysis experiments, as such the accuracy of the model depends on the accuracy of the speciation data. The measurement uncertainties of  $\text{C}_2\text{H}_4$  and  $\text{CH}_4$  are typically around 20%. Here, we carried out sensitivity analyses for the ignition delay time and flame speed with respect to the uncertainties of the measured species concentrations using the A2 model as the example. Such an analysis is not straightforward. We have to rely on a Monte Carlo approach using the following procedure:

- (1) As described in Section 3, the ratio parameters  $\lambda$ 's and  $\chi$  can be estimated directly from the (oxidative) pyrolysis in flow reactor, while parameters  $\alpha$ ,  $\beta$ , and  $\gamma$  must be determined by shock tube  $\text{C}_2\text{H}_4$  and  $\text{CH}_4$  time history data. These stoichiometric parameters, and especially  $\alpha$  and  $\beta$  determine the  $\text{C}_2\text{H}_4$  and  $\text{CH}_4$  production rates.
- (2) We estimate the bounds of  $\lambda$ 's and  $\chi$  using the scatters in the flow reactor experiments. As discussed in Section 3, the  $\gamma$  value should be close to zero. The limits of  $\gamma$  may be set to be from 0 to 2 times the  $\gamma$  value adopted in the A2 model. The limits of  $\alpha$  and  $\beta$  are set to be their mathematical bounds shown in Table 1. A Monte Carlo sample of HyChem models was generated by randomly perturbing the seven stoichiometric parameters within their respective bounds.  $\text{C}_2\text{H}_4$  and  $\text{CH}_4$  time histories were then computed at 1050, 1100, 1200, 1300, and 1400 K under the conditions of Fig. 4. The sample models were down-selected by rejecting samples with computed  $\text{C}_2\text{H}_4$  and  $\text{CH}_4$  time history profiles that lie outside the 20% upper and lower bounds of the nominal predictions of the model.
- (3) The ignition delay time and laminar flame speed were then computed using the down-selected models.

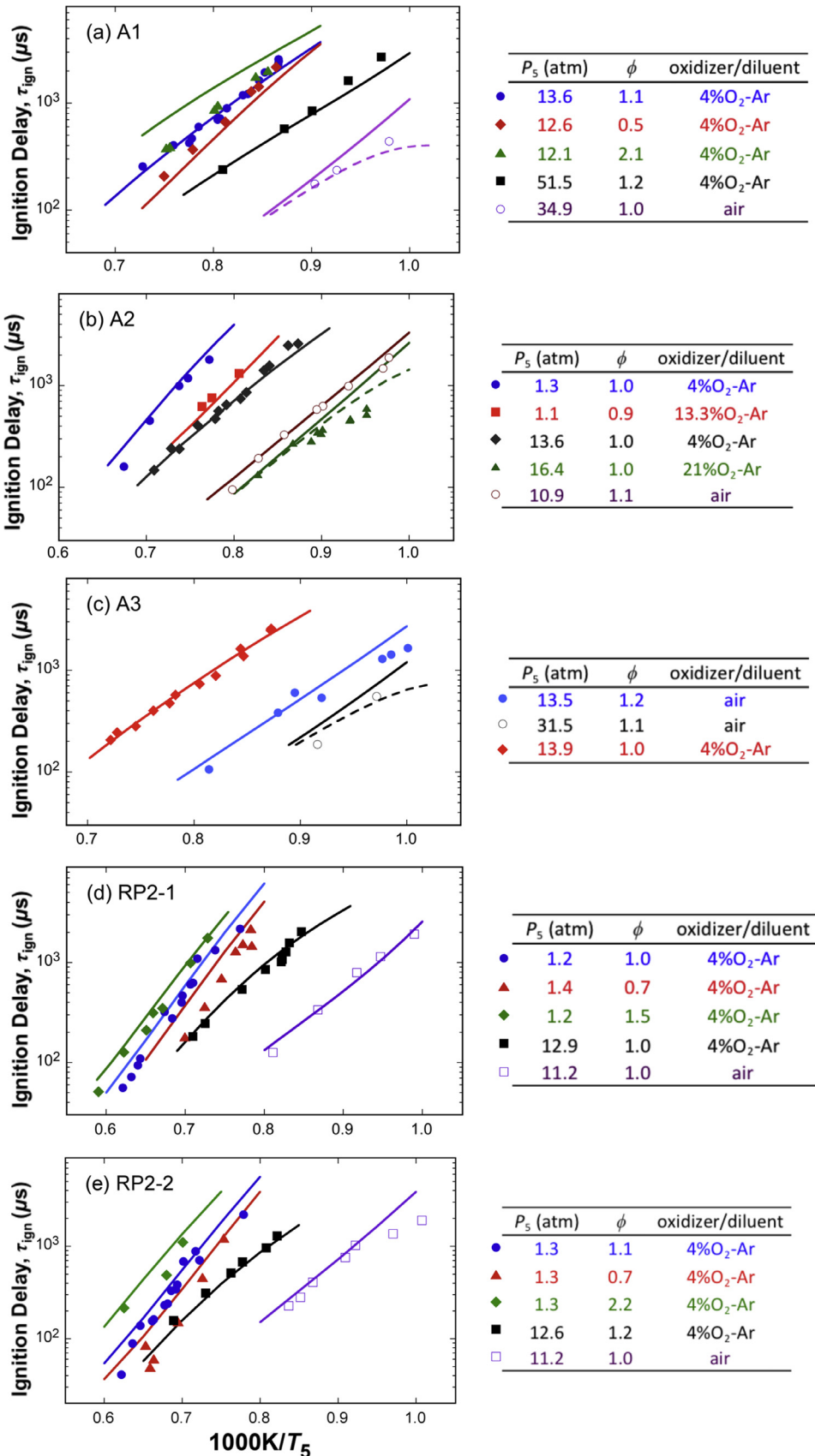


**Fig. 10.** Measured (symbols) and simulated (solid lines) ignition delay times of the A1 (a), A2 (b), A3 (c), RP2-1 (d), RP2-2 (e) under various mixture conditions. The simulations using the NTC enabled HyChem models (dashed lines) are also included in panels (a-c).

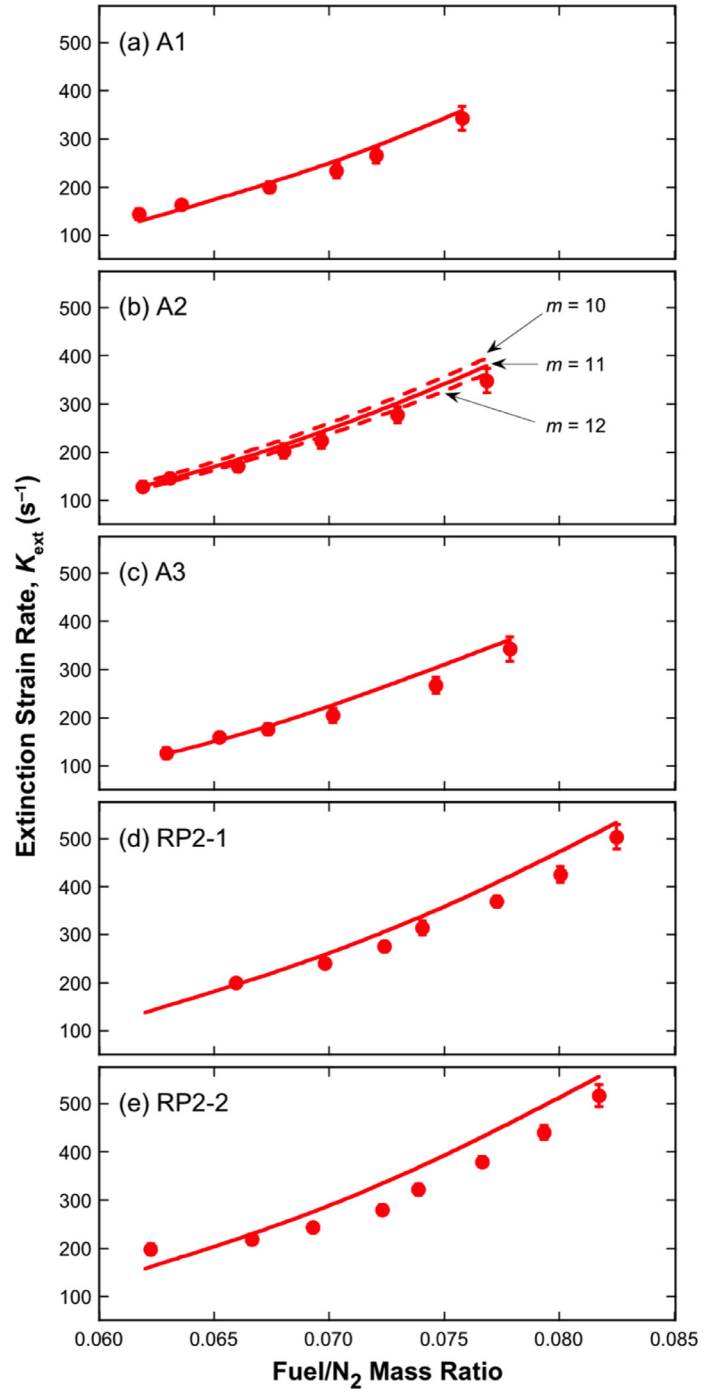
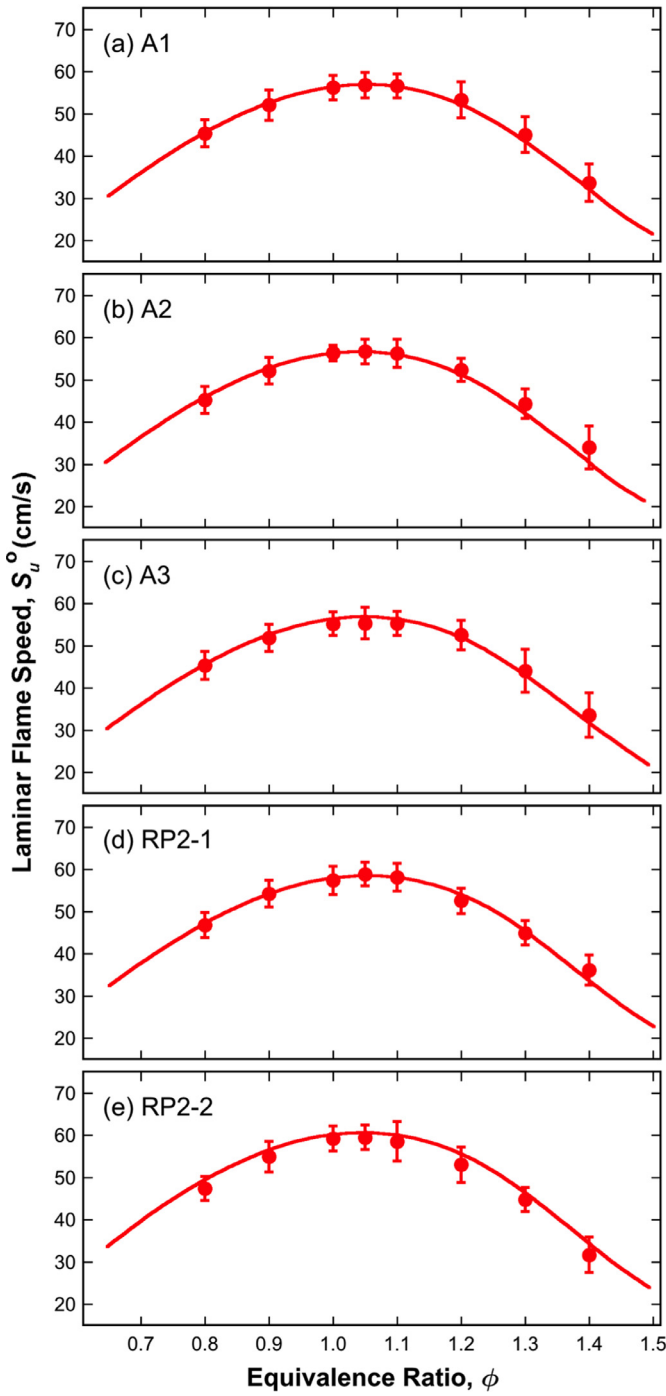


**Fig. 11.** Experimental (symbols) and simulated (lines) laminar flame speed of fuels in air at 403 K unburned gas temperature (left panel) and extinction strain rate of non-premixed fuel/N<sub>2</sub> against O<sub>2</sub> with the fuel/N<sub>2</sub> jet temperature at 473 K and O<sub>2</sub> temperature at 300 K (right panel).

Figure 14(a) shows the impact of the 20% measurement uncertainties of C<sub>2</sub>H<sub>4</sub> and CH<sub>4</sub> on ignition delay time predictions for A2 in air at an equivalence ratio of 1.1 and 10.9 atm pressure. For the condition considered the uncertainties in the species measurements translate to a model prediction uncertainty of 50% at 1000 K, which decreases to < 20% at 1200 K and becomes negligible at 1400 K. Figure 14(b) shows the result of a similar analysis for the laminar flame speed. It is seen that the species measurement uncertainty has little to no impact on the flame speed prediction. Clearly, the lack of sensitivity stems from the fact that the heat release rate is largely determined by primary chain branching and CO-to-CO<sub>2</sub> conversion reactions, and not by fuel specific reactions.

#### 5.4. The impact of foundational fuel chemistry model uncertainties

In fact, uncertainties in the foundational fuel chemistry model (i.e., USC Mech II) have a much larger impact on HyChem model accuracy. Again by Monte Carlo analysis, we generated 1000 reaction models, keeping the fuel pyrolysis part of the model as it is while sampling the uncertainty of the rate parameters in USC Mech II. The uncertainty factors were taken from Sheen et al. [46]. The logarithm of each reaction rate was assumed to be randomly perturbed under Gaussian distribution with the uncertainty factor interpreted as the 2-standard deviation. The results are shown in Fig. 15, again for the A2 fuel under conditions identical to those

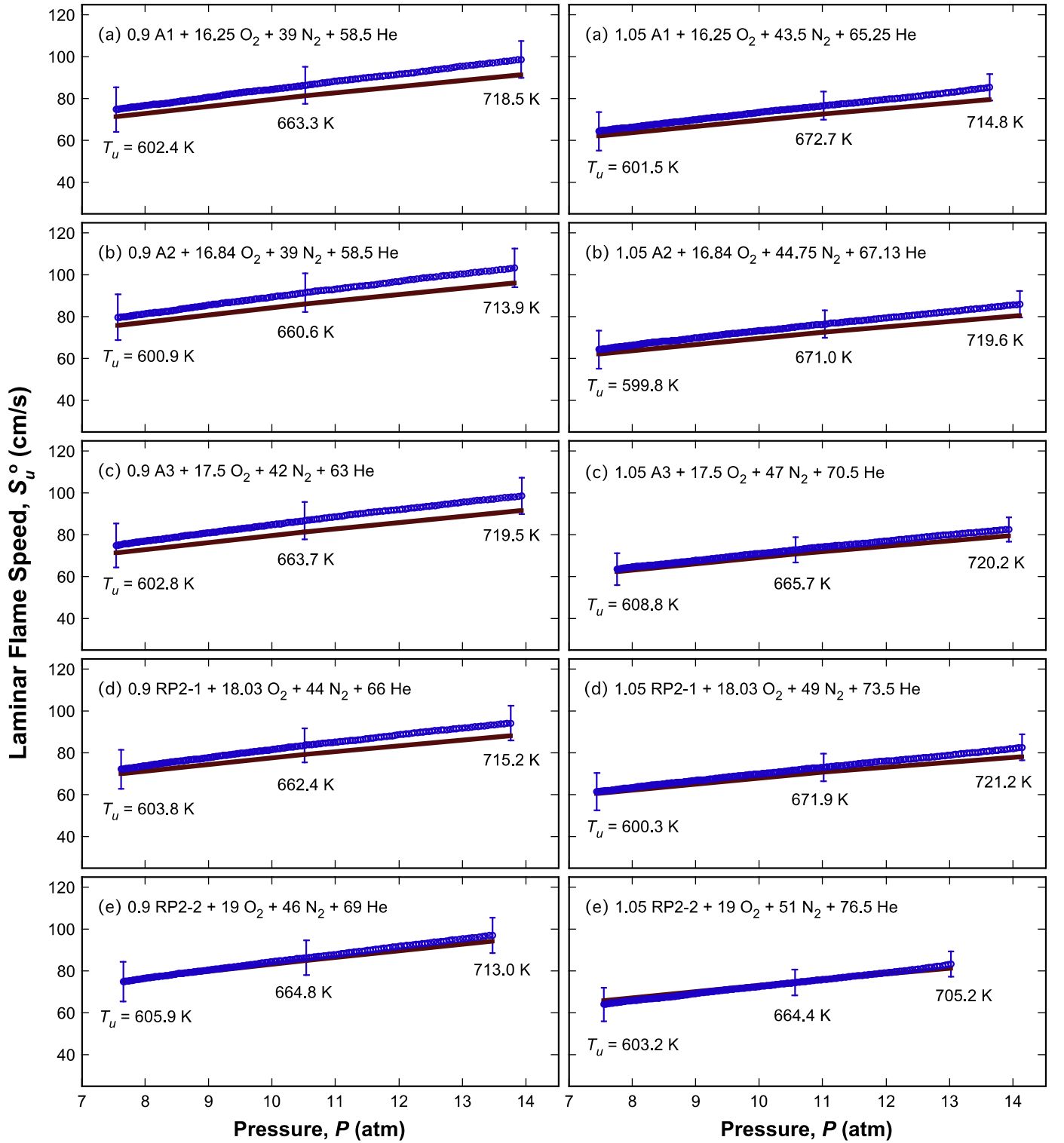


**Fig. 12.** Experimental (symbols) and simulated (lines) laminar flame speed of A1 (a), A2 (b), A3 (c), RP2-1 (d), and RP2-2 (e) in  $O_2$  at an equivalence ratio of 0.9 (left panels) and 1.05 (right panels) with  $N_2$  and He as the diluent gas at elevated pressures. The temperature values given in the plots are the unburned gas temperatures at the corresponding pressures. The error bars represent  $\pm 2\sigma$  data uncertainties.

of Fig. 14. It is seen that for both the ignition delay and laminar flame speed and under conditions chosen, the bands due to the uncertainties of USC Mech II are far larger than the respective bands due to the 20% uncertainties for the shock tube species measurements from which the fuel pyrolysis submodel was derived. Clearly, further improvement of the accuracy of the HyChem model

lies largely in the improvement of its foundational fuel submodel. This finding is consistent with many of the previous findings summarized in Ref. [47]. Additionally, the parameters of the fuel pyrolysis submodel are tightly coupled with the foundational fuel model parameters. For this reason, the current fuel pyrolysis submodel probably can be used only with USC Mech II for it to be predictive.

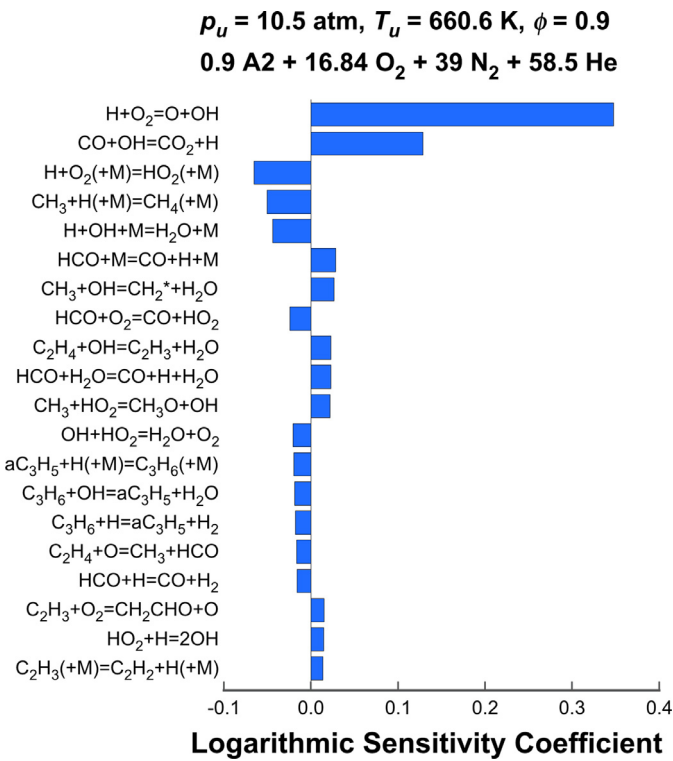


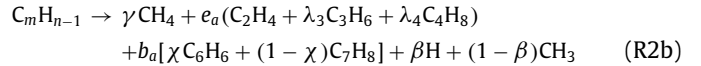
**Fig. 13.** Ranked logarithmic sensitivity coefficients of the laminar flame speed of A2 at an equivalence ratio of 0.9, 10.5 atm pressure and 660.6 K unburned gas temperature.

### 5.5. Model extension to the NTC region

Since our initial effort in advancing the HyChem approach as an alternative to the existing surrogate fuel approach, arguments have been made that the HyChem approach could not be useful to describe the NTC chemistry of the fuel. Here, we discuss an initial effort that can potentially extend the approach to cover the NTC chemistry. In fact, a form of lumped reaction model has previously been proposed by Bikas and Peters [48]. The model captures the key physics of the NTC chemistry, namely the com-

petition for QOOH, leading to effective chain termination and chain branching. Here, we follow the same approach and explore the question what should be measured in order to establish a more direct cause-and-effect relationship. We postulate that the cause is the intermediate species produced, and the effect is the NTC-chemistry dominated ignition delay we wish to predict. The results to be shown should be considered to be tentative as the approach remains empirical and is not a physics-based treatment yet. Additional studies are required to explore the validity of the approach and results presented herein.

Reaction (R2) lumps the H-abstraction of “fuel molecule” with its subsequent  $\beta$ -scission. Toward the NTC region, the  $\beta$ -scission becomes slow. Consequently, reaction (R2) is de-lumped here into two separate steps:



where  $R = \text{H}, \text{CH}_3, \text{O}_2, \text{O}, \text{OH}$ , and  $\text{HO}_2$ . The reaction rate coefficients of (R2a) are set to be equal to those of reaction (R2). The rate parameters of (R2b) are assumed to be equal to the sum of the  $\beta$ -scission rates of an equilibrated population of all *n*-dodecyl radical isomers. These changes do not affect HyChem model predictions for the high-temperature data discussed thus far. The NTC and low-temperature chemistry submodel is introduced as follows:

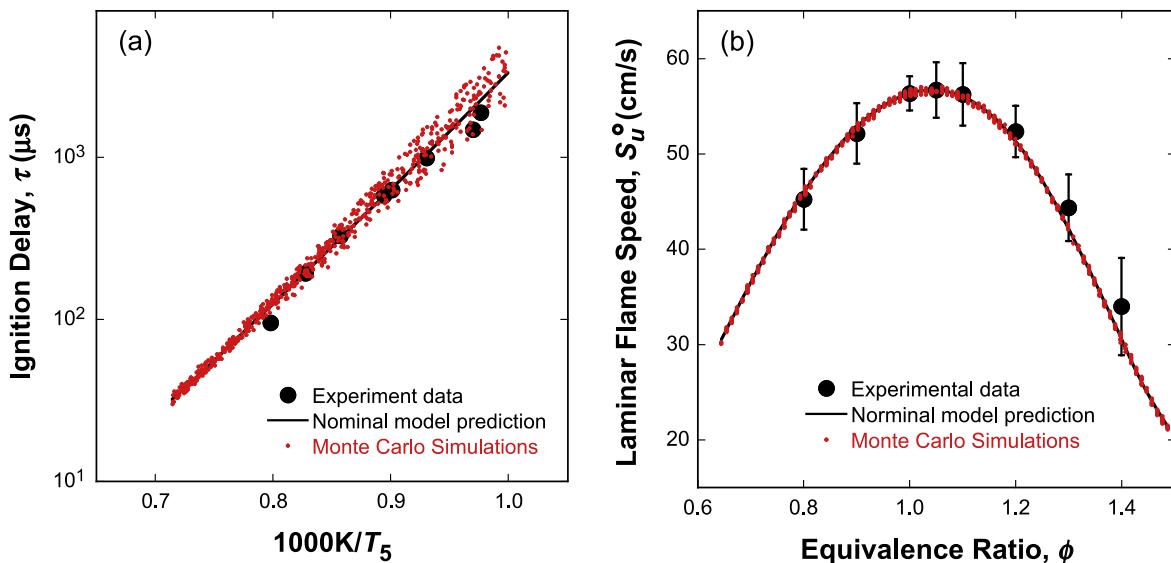
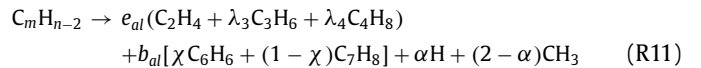
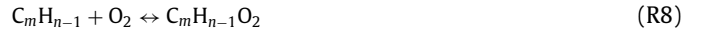


**Fig. 14.** Sensitivity of (a) predicted ignition delay time of A2 in air at an equivalence ratio of 1.1 and a pressure of 10.9 atm and (b) predicted laminar flame speed of A2 in air at the pressure of 1 atm and unburned gas temperature of 403 K with respect to the measurement uncertainties of  $\text{C}_2\text{H}_4$  and  $\text{CH}_4$  concentration, each at 20%.

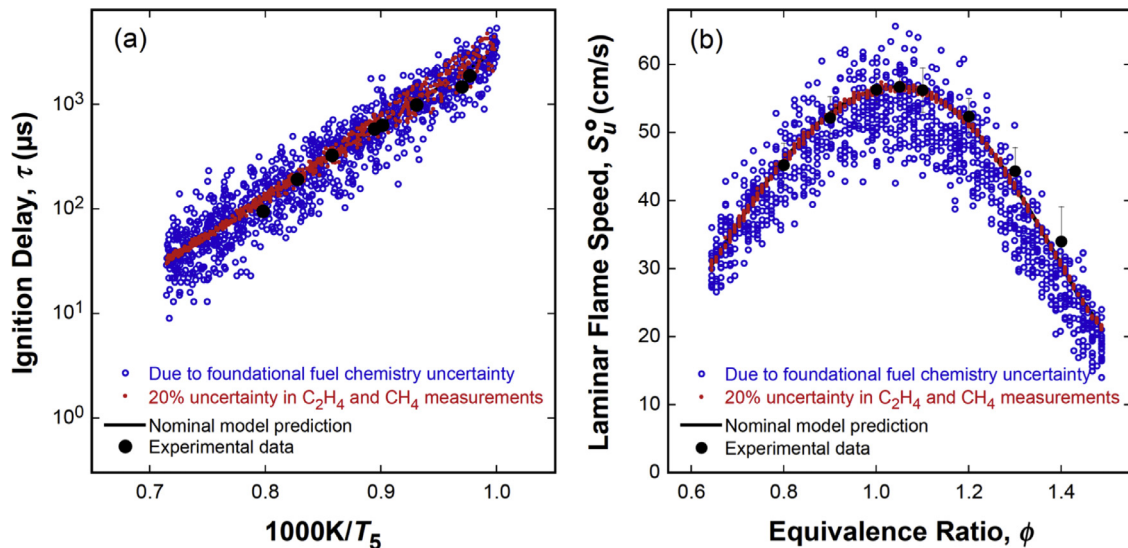
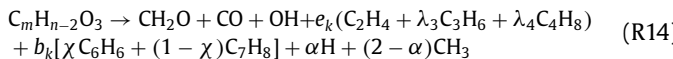


**Fig. 15.** Sensitivity of HyChem model predictions of (a) ignition delay time of A2/air mixture at 1.1 equivalence ratio and 10.9 atm pressure, and (b) A2/air laminar flame speed at 1 atm pressure and 403 K unburned gas temperature.



The addition of  $\text{O}_2$  to the “fuel radical” produces the peroxy radical (R8), which isomerizes to the QOOH radical via H-atom shift. An increase in temperature causes R9 to proceed in the back direction, thus impeding chain branching in the NTC region. The hydroperoxy radical ( $\text{C}_m\text{H}_{n-2}\text{OOH}$  or QOOH) either decomposes to the unreactive  $\text{HO}_2$  radical and the alkene form of the “fuel molecule,” or reacts with  $\text{O}_2$  to form  $\text{C}_m\text{H}_{n-1}\text{O}_4$  (OOQOOH) (R12). The dissociation of OOQOOH produces the net chain branching effect by yielding the OH radical and ketohydroperoxide ( $\text{C}_m\text{H}_{n-2}\text{O}_3$  or QOOH). The dissociation of the ketohydroperoxide (R14) is treated in the similar manner as the fuel-derived alkene  $\text{C}_m\text{H}_{n-2}$ . They both decompose following the similar treatment of reaction (R1). Additional reactions could be included as needed, but for now this is unnecessary as the ignition delay appears to be sensitive to the rates of a very few reactions.

The thermochemical data of the pseudo-species, including  $\text{C}_m\text{H}_{n-1}\text{O}_2$ ,  $\text{C}_m\text{H}_{n-2}\text{OOH}$ ,  $\text{C}_m\text{H}_{n-1}\text{O}_4$  and  $\text{C}_m\text{H}_{n-2}\text{O}_3$ , were estimated by the group additivity method. For example, the property value of  $\text{C}_{12}\text{H}_{22}\text{O}_2$  (derived from the A3 fuel) was obtained from the thermochemical property values of the parent fuel, *n*-dodecane, and its peroxy radical:

$$P(\text{C}_{12}\text{H}_{22}\text{O}_2) = P(\text{A3}, \text{C}_{12}\text{H}_{23}) + P(\text{C}_{12}\text{H}_{25}\text{O}_2) - P(\text{n-C}_{12}\text{H}_{26})$$

where  $P$  denotes the enthalpy of formation and entropy at the standard state and specific heats. The rate parameters were initially adopted from those of *n*-dodecane low-temperature oxidation model in JetSurF 1.0 [30], and the proposed NTC-submodels are available in the Supplementary Materials for A1, A2 and A3 fuels. Selected rate parameters ( $k_8$  and  $k_{14}$ ) were adjusted within a factor of 5 from those used in JetSurF 1.0 to match the ignition delay time measured under a nominal pressure of 12 atm and tested against data at around 35 atm for A1 and 31 atm for A3 to a limited extent because of limited test data, as shown in Fig. 16. Because the derived cetane numbers (DCNs) of A1 (48.8) and A2 (48.3) are nearly equal, the submodels of these two fuels are

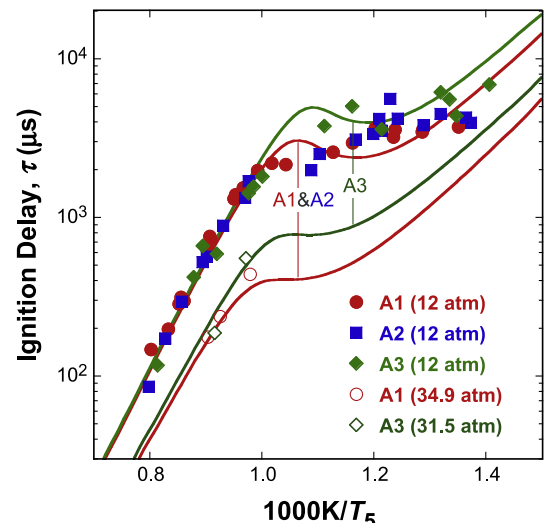


**Fig. 16.** Comparison of measured (symbols) and computed (lines) ignition delay times of A1, A2, and A3 in air at varying nominal pressures and unity equivalence ratio. The predicted ignition delays overlap between A1 and A2.

indistinguishable. The DCN of A3 is smaller and equal to 39.2 [21] and experimentally A3 exhibits somewhat slower oxidation chemistry in the low-temperature region. Here, it is useful to note that the DCN of typical jet fuels ranges from 40 to 60 [21]. Hence, the A3 fuel sets the lower bound for the NTC activities, while the NTC activities of A1 and A2 represent the average of jet fuels.

As Fig. 16 shows, the measured and simulated ignition delay times agree with each other well. Although we have only limited data above 30 atm and the rate parameters of the NTC submodel was only adjusted against data at 12 atm, the NTC-enabled HyChem model appears to capture the data at 31 and 35 atm. Our unpublished work on gasoline fuels provides more direct evidence that supports the extrapolative capability of the NTC-enabled HyChem over a wide range of pressure. In that study, it was shown clearly that the rate parameters fitted to ignition delay data at 15 atm in a manner similar to the current study allow the reaction model to reproduce the ignition delay data at 35 and 60 atm. The

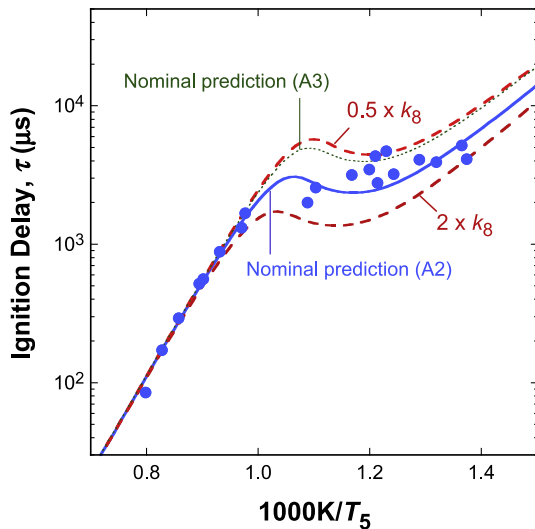


**Fig. 17.** Comparison of measured (symbols) and simulated (solid line) ignition delay time of A2 in air at the nominal pressure of 12.0 atm and unity equivalence ratio. The dashed lines indicate  $k_8$  sensitivity for A2, and dotted line is nominal prediction for A3.

discussion about gasoline fuels is, however, beyond the scope of the current paper.

From a fundamental standpoint, fitting the model parameters against the ignition delay is far less than satisfactory. In the realm of the HyChem approach, the key question is what species time histories are required to inverse the problem. For the high-temperature chemistry, our approach was to seek for the direct cause and effect and devise a model to establish the causal relationship via the measurement of the distribution of the small intermediate species from fuel decomposition and their production rates, as these are the most critical factors impacting a wide range of combustion phenomena. For the NTC chemistry of real fuels, we explore a similar approach here using the NTC-enabled model as the starting point of our analysis.

While the key marker of the NTC activities is the  $C_mH_{n-2}OOH$  or QOOH radical, the ignition delay time is the most sensitive to  $k_8$ , i.e., the rate coefficient of  $O_2$  addition to the fuel radical

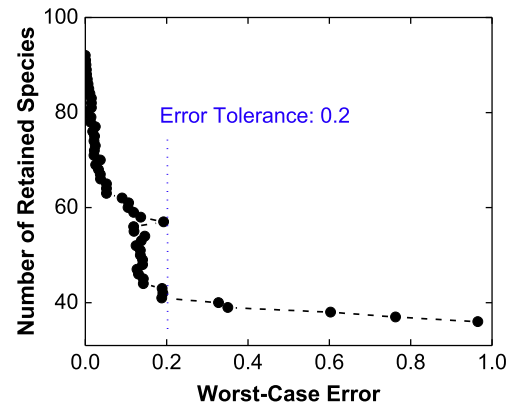


**Fig. 19.** Accumulative worst-case error in the target parameters in sensitivity analysis as a function of the number of retained species in the skeletal model for A2.

$C_mH_{n-1}$  and to the equilibrium constant of the same reaction. To illustrate this point, we plot in Fig. 17 the  $2 \times k_8$  and  $0.5 \times k_8$  sensitivities of the A2 model against the experimental data of A2 in air at 12 atm. It is seen that a change in  $k_8$  by a factor of 2 impacts the NTC ignition delay time by roughly a factor of 2. Interestingly, these two cases are expected to bracket the NTC activities of typical jet fuels. As seen,  $0.5 \times k_8$  yields the ignition delay times close to those of A3, whose DCN lies at the lower limit of typical jet fuels. The A2 fuel represents the average of the NTC activities of available jet fuels with a DCN of 48. It is therefore reasonable to speculate that the highest NTC activity can be represented quite closely by the  $2 \times k_8$  case, which should represent a fuel with DCN  $\sim 60$ . Over the available range of DCN of the jet fuels, the variation of the time history of the key NTC marker, the QOOH, is large, as shown in the left panel of Fig. 18. Since the NTC chemistry is largely sensitive to the rate of R8 only, the time history of QOOH is probably sufficient to determine  $k_8$  if QOOH can be reliably measured by laser diagnostics. The unfortunate factor is that its concentration is at a sub-ppm level; and this presents tremendous diagnostic challenges especially when Q represents a range of chemical functionalities that cannot be determined confidently.

In fact, as the product of the NTC reactions, formaldehyde ( $CH_2O$ ) is perhaps the best NTC marker. The time histories of

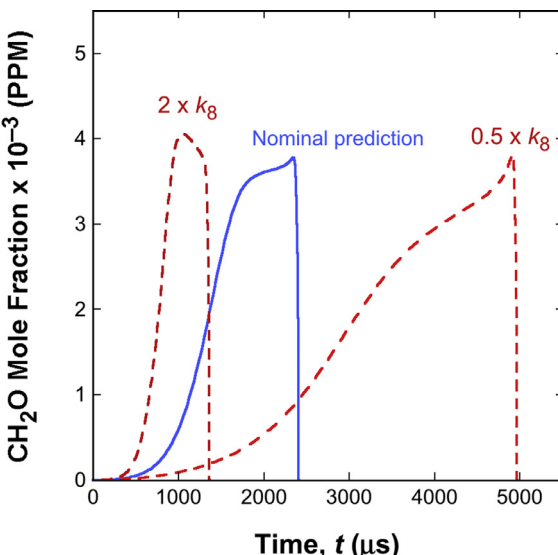
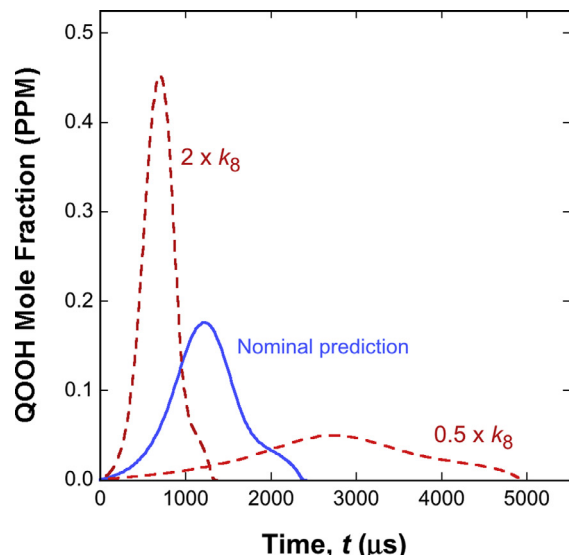


**Fig. 18.** Simulated  $C_mH_{n-2}OOH$  (QOOH) (left panel) and  $CH_2O$  (right panel) time histories at  $T_5 = 875$  K under otherwise the condition of A2 oxidation same as shown in Fig. 17.

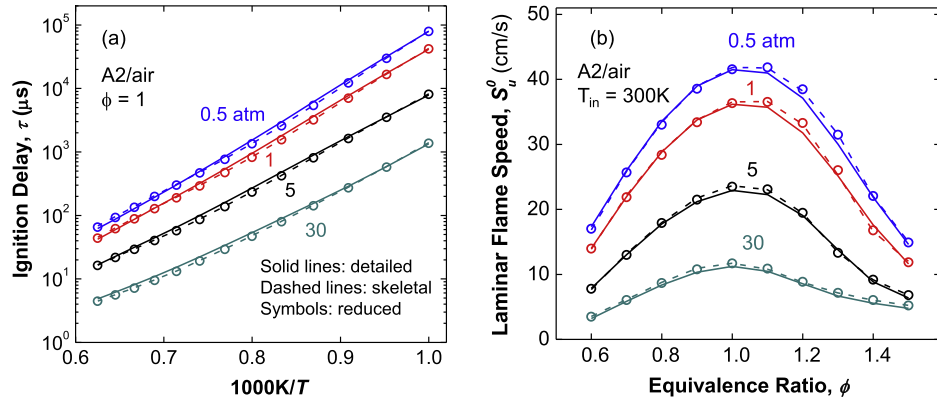


**Fig. 20.** (a) Ignition delay and (b) laminar flame speed at different pressures for the A2/air, calculated with the detailed, skeletal and reduced models, respectively.

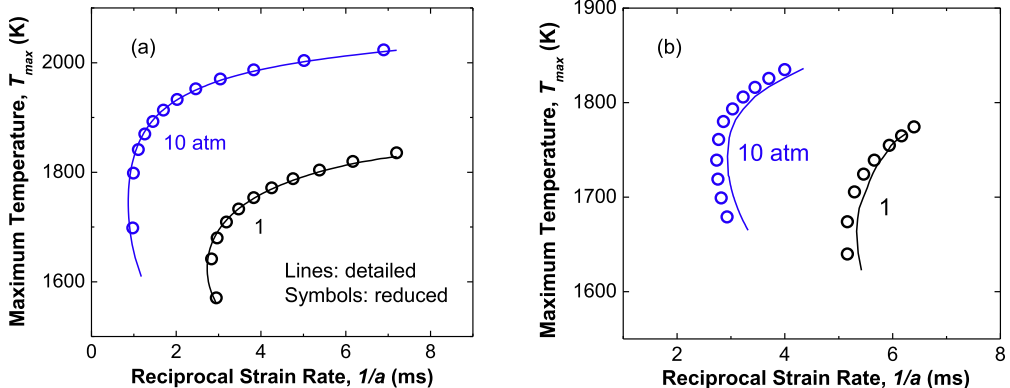


**Fig. 21.** Maximum temperature in (a) non-premixed counterflow flames of  $\text{N}_2$ -diluted A2 (50% in mole) opposed to air with inlet temperatures of 300 K, and (b) counterflow premixed flames with equivalence ratio of 0.7 and free-stream temperature of 300 K, as function of the reciprocal strain rate, calculated with the detailed and reduced models, respectively.

$\text{CH}_2\text{O}$  are presented in the right panel of Fig. 18, showing again the strong sensitivity in shape and concentration growth rate to  $k_8$ . The concentration of  $\text{CH}_2\text{O}$  reaches the level of a few thousand ppm, making it a viable measurement target and key marker for unraveling and characterizing the NTC behaviors of jet fuels. We note that laser diagnostics of  $\text{CH}_2\text{O}$  in shock tube is a well-developed technique [49–51].

### 5.6. Skeletal and reduced models

Excluding the NTC submodel, each HyChem model consists of 119 species and 841 reactions. While these modes are already reduced in size compared to other existing models for large hydrocarbon fuels, they can be reduced further in size as will be discussed in this section using the A2 model as an example. The skeletal and reduced models can be found also in the Supplementary Materials.

Model reduction is based on reaction states sampled from auto-ignition and perfectly stirred reactors (PSR). The reduction parameter range covers pressure of 0.5–30 atm, equivalence ratio of 0.5–1.5, initial temperature of 1000–1600 K for auto-ignition, and inlet temperature of 300 K for PSR. Skeletal reduction with directed relation graph (DRG) [52] and sensitivity analysis [53] was first applied to eliminate unimportant species and reactions from the HyChem models. In DRG, the H atom is selected as the starting species using an error threshold of 0.3. After the skeletal reduction, the resulting skeletal models are further reduced with

sensitivity analysis with ignition delay and extinction residence time of PSR as the target parameters.

Figure 19 shows the accumulative worst-case relative error in the target parameters as a function of the number of retained species in the skeletal model. The vertical, dotted line indicates the prescribed error threshold in the sensitivity analysis, which is 20% for A2 fuel, chosen at the onset of the rapid deterioration of the model quality as exhibited in the rapid increase in the worst-case error of the target parameters. The final skeletal model consists of 41 species. As the last step in the skeletal reduction, reactions unimportant for all the retained species were removed by comparing the contribution of each reaction to each retained species using an error threshold of 20% [54]. In the second-stage of the reduction, linearized quasi-steady-state approximations (LQSSA) [55] are applied on 10 quasi-steady-state (QSS) species. The QSS species are removed from the transport equations and are analytically solved using internal algebraic equations with a graph-based method [55]. Hence, the final reduced model contains 31 species. Application of the reduced models requires the use of model-specific subroutines for rate evaluation. The Chemkin-compatible routines are provided in the Supplementary Materials for all five fuels, through a webpage link.

Figure 20 shows selected test results of the reduced and skeletal models for ignition delay and laminar flame speed. The reduced and skeletal models agree well with the original HyChem models over the conditions tested. Fig. 21 compares the maximum flame temperature as a function of the reciprocal strain rate for non-premixed and premixed flames. Again, the reduced models

agree well with the original HyChem models including the turning points, with the worst-case relative error being approximately 15%.

## 6. Conclusions

The HyChem (hybrid chemistry) approach was demonstrated for three aviation and two rocket fuels. Specifically, HyChem models were developed using advanced speciation data in shock tubes, which are supplemented by similar data from a flow reactor. For these fuels, key species to consider are  $C_2H_4$ ,  $CH_4$ ,  $C_3H_6$ , 1- $C_4H_8$ ,  $i-C_4H_8$ , benzene and toluene with  $C_2H_4$  and  $CH_4$  being the two most important species for all of the fuels considered. It is shown that the reaction rate coefficients and stoichiometric parameters can be jointly determined by matching the species time histories from shock tube and flow reactor (oxidative) pyrolysis experiments. While work is still ongoing to identify an optimal set of experiments for the development of the fuel pyrolytic submodel, the HyChem models are shown to predict the global combustion properties, including ignition delay time, laminar flame speed under both atmospheric and elevated pressures, and non-premixed extinction strain rates rather well for the five fuels tested. In most cases, the models reproduce the data within their uncertainties.

The sensitivities of model predictions to the measurement uncertainty of  $C_2H_4$  and  $CH_4$  in shock tubes were examined. The results show that the 20% uncertainties in the measurement of the two species are by no means severe. For example, when these uncertainties are propagated into global combustion property predictions, the impact is negligible for the laminar flame speed and 20% uncertainty for ignition delay at an initial temperature of 1200 K and pressure of 10.9 atm. In contrast, the impact of the uncertainties in the foundational fuel chemistry model (USC Mech II) far exceeds that of the uncertainties in the fuel pyrolytic submodel, and as such future studies should be directed at reducing the uncertainties in the key kinetic parameters in the foundational fuel chemistry model.

NTC-enabled HyChem models and an approach to low-temperature chemistry modeling are proposed. Within the realm of the HyChem approach,  $CH_2O$  is the most suitable marker for the NTC behavior and thus the most critical species to measure experimentally in that region. Finally, it is shown that for all five fuels tested, each of the HyChem models can be reduced to a compact skeletal model with about 40 and a reduced model with about 30 species. While this number of species may still be too large for use in some of the computational fluid dynamics (CFD) simulations, the advance of these models represents a significant progress, bringing the use of reaction models of real fuels in CFD simulations a step closer.

Lastly, the efficiency and accuracy of the HyChem approach discussed herein and the removal of the difficulties associated with mismatched reaction kinetics and spray modeling demonstrate the fact that the HyChem approach is preferable to the surrogate fuel approach as a tangible solution to the real-fuel combustion chemistry problem.

## Acknowledgment

The significant technical involvement by the AFOSR program manager, Dr. Chiping Li, is acknowledged. This research was funded by the Air Force Office of Scientific Research under grant numbers FA9550-14-1-0235 (CTB, RKH and HW), FA9550-16-1-0195 (CTB, RKH and HW), FA9550-15-1-0409 (FNE), FA9550-15-1-0496 (TL), and FA9550-16-1-0079 (KB). The work was also supported by the National Aeronautics and Space Administration (NASA) under agreement numbers NNX15AV05A (HW) and NNX15AU96A (TL) and by the Federal Aviation Administration Office of Environment and Energy as a part of ASCENT Projects 26 and 35 under

FAA Award Numbers 13-CAJFE-SU-006 (HW) and 13-C-AJFE-SU-016 (RKH). Any opinions, findings, and conclusions or recommendations expressed in this material are those of the authors and do not necessarily reflect the views of the FAA or other ASCENT sponsors.

## Supplementary materials

Supplementary material associated with this article can be found, in the online version, at doi:10.1016/j.combustflame.2018.03.021.

## References

- [1] A. Violi, S. Yan, E. Eddings, A. Sarofim, S. Granata, T. Faravelli, E. Ranzi, Experimental formulation and kinetic model for JP-8 surrogate mixtures, Combust. Sci. Technol. 174 (2002) 399–417.
- [2] M. Colket, T. Edwards, S. Williams, N.P. Cernansky, D.L. Miller, F. Egolfopoulos, P. Lindstedt, K. Seshadri, F.L. Dryer, C.K. Law, Development of an experimental database and kinetic models for surrogate jet fuels, 45<sup>th</sup> AIAA Aerospace Sciences Meeting and Exhibit, Reno, NV, (2007) AIAA Paper No. 2007-770.
- [3] E.G. Eddings, S. Yan, W. Ciro, A.F. Sarofim, Formulation of a surrogate for the simulation of jet fuel pool fires, Combust. Sci. Technol. 177 (2005) 715–739.
- [4] H.R. Zhang, E.G. Eddings, A.F. Sarofim, Criteria for selection of components for surrogates of natural gas and transportation fuels, Proc. Combust. Inst. 31 (2007) 401–409.
- [5] M. Colket, T. Edwards, S. Williams, N.P. Cernansky, D.L. Miller, F. Egolfopoulos, F.L. Dryer, J. Bellan, P. Lindstedt, K. Seshadri, Identification of target validation data for development of surrogate jet fuels, 46<sup>th</sup> AIAA, Aerospace Sciences Meeting and Exhibit, Reno, NV, (2008) AIAA Paper No. 2008-972.
- [6] S. Dooley, S.H. Won, M. Chaos, J. Heyne, Y. Ju, F.L. Dryer, K. Kumar, C.-J. Sung, H. Wang, M.A. Oehlschlaeger, A jet fuel surrogate formulated by real fuel properties, Combust. Flame 157 (2010) 2333–2339.
- [7] J. Farrell, N. P. Cernansky, F. L. Dryer, C. K. Law, D. Friend, C. Hergart, R. McDavid, A. Patel, C.J. Mueller, H. Pitsch, Development of an experimental database and kinetic models for surrogate diesel fuels, SAE Technical Paper No. 2007-01-0201 (2007).
- [8] S. Dooley, S.H. Won, J. Heyne, T.I. Farouk, Y. Ju, F.L. Dryer, K. Kumar, X. Hui, C.-J. Sung, H. Wang, The experimental evaluation of a methodology for surrogate fuel formulation to emulate gas phase combustion kinetic phenomena, Combust. Flame 159 (2012) 1444–1466.
- [9] S. Dooley, S.H. Won, S. Jahangirian, Y. Ju, F.L. Dryer, H. Wang, M.A. Oehlschlaeger, The combustion kinetics of a synthetic paraffinic jet aviation fuel and a fundamentally formulated, experimentally validated surrogate fuel, Combust. Flame 159 (2012) 3014–3020.
- [10] F.L. Dryer, S. Jahangirian, S. Dooley, S.H. Won, J. Heyne, V.R. Iyer, T.A. Litzinger, R.J. Santoro, Emulating the combustion behavior of real jet aviation fuels by surrogate mixtures of hydrocarbon fluid blends: implications for science and engineering, Energy Fuel 28 (2014) 3474–3485.
- [11] H. Wang, R. Xu, K. Wang, C.T. Bowman, D.F. Davidson, R.K. Hanson, K. Brezinsky, F.N. Egolfopoulos, A Physics-based approach to modeling real-fuel combustion chemistry - I. Evidence from experiments, and thermodynamic, chemical kinetic and statistical considerations, Combust. Flame (2017), doi:10.1016/j.combustflame.2018.03.019.
- [12] D. F. Davidson, Y. Zhu, J. Shao, R. K. Hanson, Ignition delay time correlations for distillate fuels, Fuel 187 (2017) 26–32.
- [13] T. Parise, D. F. Davidson, R. K. Hanson, Shock tube/laser absorption measurements of the pyrolysis of a bimodal test fuel, Proc. Combust. Inst. 36 (2017) 281–288.
- [14] A. Fridlyand, K. Brezinsky, A. Mandelbaum, *n*-Heptane pyrolysis and oxidation in ethylene-methane and iso-octane mixtures, J. Propuls. Power 29 (2013) 732–743.
- [15] W. Tang, K. Brezinsky, Chemical kinetic simulations behind reflected shock waves, Int. J. Chem. Kinet. 38 (2006) 75–97.
- [16] S. Banerjee, R. Tangko, D.A. Sheen, H. Wang, C.T. Bowman, An experimental and kinetic modeling study of *n*-dodecane pyrolysis and oxidation, Combust. Flame 163 (2016) 12–30.
- [17] Y. Wang, A. Holley, C. Ji, F. N. Egolfopoulos, T. Tsotsis, H. Curran, Propagation and extinction of premixed dimethyl-ether/air flames, Proc. Combust. Inst. 32 (2009) 1035–1042.
- [18] C. Xiouris, T. Ye, J. Jayachandran, F.N. Egolfopoulos, Laminar flame speeds under engine-relevant conditions: uncertainty quantification and minimization in spherically expanding flame experiments, Combust. Flame 163 (2016) 270–283.
- [19] H. Wang, X. You, A.V. Joshi, S.G. Davis, A. Laskin, F. Egolfopoulos, C.K. Law, USC Mech Version II. High-Temperature Combustion Reaction Model of  $H_2/CO/C_1-C_4$  Compounds. [http://ignis.usc.edu/USC\\_Mech\\_II.htm](http://ignis.usc.edu/USC_Mech_II.htm), 2007.
- [20] M. Colket, J. Heyne, M. Rumizen, M. Gupta, T. Edwards, W.M. Roquemore, G. Andac, R. Boehm, J. Lovett, R. Williams, Overview of the national jet fuels combustion program, AIAA J. 55 (2017) 1087–1104.
- [21] T. Edwards, Personal communication, (2015).
- [22] R.J. Kee, F.M. Rupley, J.A. Miller, CHEMKIN: a general-purpose, problem-independent, transportable, FORTRAN chemical kinetics code package, Sandia National Laboratories, Albuquerque, N.M., 1989 Sandia Report SAND-89-8009.

- [23] R.J. Kee, J.F. Grcar, M.D. Smooke, J. Miller, E. Meeks, PREMIX: a Fortran program for modeling steady laminar one-dimensional premixed flames, Sandia National Laboratories, Albuquerque, N.M., 1985 Sandia Report SAND85-8240.
- [24] F. Egolfopoulos, Geometric and radiation effects on steady and unsteady strained laminar flames, Symp. (Int.) Combust. 25 (1994) 1375–1381.
- [25] R.J. Kee, J.A. Miller, G.H. Evans, G. Dixon-Lewis, A computational model of the structure and extinction of strained, opposed flow, premixed methane-air flames, Symp. (Int.) Combust. 22 (1989) 1479–1494.
- [26] M. Nishioka, C. K. Law, T. Takeno, A flame-controlling continuation method for generating S-curve responses with detailed chemistry, Combust. Flame 104 (1996) 328–342.
- [27] C. Liu, Z. Li, H. Wang, Drag force and transport property of a small cylinder in free molecule flow: a gas-kinetic theory analysis, Phys. Rev. E 94 (2016) 023102.
- [28] C. Liu, W.S. McGivern, J.A. Manion, H. Wang, Theory and experiment of binary diffusion coefficient of *n*-alkanes in dilute gases, J. Phys. Chem. A 120 (2016) 8065–8074.
- [29] C. Liu, R. Zhao, R. Xu, F.N. Egolfopoulos, H. Wang, Binary diffusion coefficients and non-premixed flames extinction of long-chain alkanes, Proc. Combust. Inst. 36 (2017) 1523–1530.
- [30] B. Sirjean, E. Dames, D.A. Sheen, X. You, C. Sung, A.T. Holley, F.N. Egolfopoulos, H. Wang, S.S. Vasu, D.F. Davidson, R.K. Hanson, H. Pitsch, C.T. Bowman, A. Kelley, C.K. Law, W. Tsang, N.P. Cernansky, D.L. Millar, A. Violi, N.P. Lindstedt, A high-temperature chemical kinetic model of *n*-alkane oxidation, JetSurF version 1.0, September 15, 2009, <http://web.stanford.edu/group/haiwanglab/JetSurF/JetSurF1.0/index.html>, 2009.
- [31] H. Wang, E. Dames, B. Sirjean, D.A. Sheen, R. Tangko, A. Violi, J.Y.W. Lai, F.N. Egolfopoulos, D.F. Davidson, R.K. Hanson, C.T. Bowman, C.K. Law, W. Tsang, N.P. Cernansky, D.L. Millar, R.P. Lindstedt, A high-temperature chemical kinetic model of *n*-alkane (up to *n*-dodecane), cyclohexane, and methyl-, ethyl-, *n*-propyl and *n*-butyl-cyclohexane oxidation at high temperatures, JetSurF version 2.0, September 19, 2010, <http://web.stanford.edu/group/haiwanglab/JetSurF/JetSurF2.0/index.html>, 2010.
- [32] A.J. Dean, O.G. Penyazkov, K.L. Sevruk, B. Varatharajan, Ignition of aviation kerosene at high temperatures. Ignition of aviation kerosene at high temperatures, 20th International Colloquium on Dynamics of Explosions and Reactive Systems, Montreal, Canada (2005) Paper No. 87.
- [33] M.S. Kahanawala, M.J. DeWitt, E. Corporan, S.S. Sidhu, Ignition and emission characteristics of surrogate and practical jet fuels, Energy Fuel 22 (2008) 3673–3679.
- [34] S.S. Vasu, D.F. Davidson, R.K. Hanson, Jet fuel ignition delay times: shock tube experiments over wide conditions and surrogate model predictions, Combust. Flame 152 (2008) 125–143.
- [35] K. Kumar, C.-J. Sung, An experimental study of the autoignition characteristics of conventional jet fuel/oxidizer mixtures: Jet-A and JP-8, Combust. Flame 157 (2010) 676–685.
- [36] D.A. Rothamer, L. Murphy, Systematic study of ignition delay for jet fuels and diesel fuel in a heavy-duty diesel engine, Proc. Combust. Inst 34 (2013) 3021–3029.
- [37] K.E. Far, F. Parsinejad, H. Metghalchi, Flame structure and laminar burning speeds of JP-8/air premixed mixtures at high temperatures and pressures, Fuel 89 (2010) 1041–1049.
- [38] C. Wu, C.K. Law, On the determination of laminar flame speeds from stretched flames, Symp. (Int.) Combust. 20 (1985) 1941–1949.
- [39] K. Kumar, C.-J. Sung, X. Hui, Laminar flame speeds and extinction limits of conventional and alternative jet fuels, Fuel 90 (2011) 1004–1011.
- [40] X. Hui, C.-J. Sung, Laminar flame speeds of transportation-relevant hydrocarbons and jet fuels at elevated temperatures and pressures, Fuel 109 (2013) 191–200.
- [41] S. Humer, A. Frassoldati, S. Granata, T. Faravelli, E. Ranzi, R. Seiser, K. Seshadri, Experimental and kinetic modeling study of combustion of JP-8, its surrogates and reference components in laminar nonpremixed flows, Proc. Combust. Inst 31 (2007) 393–400.
- [42] K. Seshadri, S. Humer, R. Seiser, Activation-energy asymptotic theory of autoignition of condensed hydrocarbon fuels in non-premixed flows with comparison to experiment, Combust. Theor. Model. 12 (2008) 831–855.
- [43] S. Humer, R. Seiser, K. Seshadri, Experimental investigation of combustion of jet fuels and surrogates in nonpremixed flows, J. Propul. Power 27 (2011) 847–855.
- [44] R.K. Gehmlich, A. Kuo, K. Seshadri, Experimental investigations of the influence of pressure on critical extinction conditions of laminar nonpremixed flames burning condensed hydrocarbon fuels, jet fuels, and surrogates, Proc. Combust. Inst. 35 (2015) 937–943.
- [45] B. Li, N. Liu, R. Zhao, F.N. Egolfopoulos, H. Zhang, Extinction studies of flames of heavy neat hydrocarbons and practical fuels, J. Propul. Power 29 (2013) 352–361.
- [46] D.A. Sheen, X. You, H. Wang, T. Løvås, Spectral uncertainty quantification, propagation and optimization of a detailed kinetic model for ethylene combustion, Proc. Combust. Inst. 32 (2009) 535–542.
- [47] H. Wang, D.A. Sheen, Combustion kinetic model uncertainty quantification, propagation and minimization, Prog. Energy Combust. Sci. 47 (2015) 1–31.
- [48] G. Bikas, N. Peters, Kinetic modelling of *n*-decane combustion and autoignition: modeling combustion of *n*-decane, Combust. Flame 126 (2001) 1456–1475.
- [49] G. Friedrichs, D.F. Davidson, R.K. Hanson, Validation of a thermal decomposition mechanism of formaldehyde by detection of CH<sub>2</sub>O and HCO behind shock waves, Int. J. Chem. Kinet. 36 (2004) 157–169.
- [50] S. Wang, D.F. Davidson, R.K. Hanson, High-temperature laser absorption diagnostics for CH<sub>2</sub>O and CH<sub>3</sub>CHO and their application to shock tube kinetic studies, Combust. Flame 160 (2013) 1930–1938.
- [51] G. Friedrichs, D.F. Davidson, R.K. Hanson, Direct measurements of the reaction H + CH<sub>2</sub>O → H<sub>2</sub> + HCO behind shock waves by means of Vis–UV detection of formaldehyde, Int. J. Chem. Kinet. 34 (2002) 374–386.
- [52] T. Lu, C.K. Law, A directed relation graph method for mechanism reduction, Proc. Combust. Inst. 30 (2005) 1333–1341.
- [53] X. Zheng, T. Lu, C.K. Law, Experimental counterflow ignition temperatures and reaction mechanisms of 1,3-butadiene, Proc. Combust. Inst. 31 (2007) 367–375.
- [54] T. Lu, C.K. Law, Strategies for mechanism reduction for large hydrocarbons: *n*-heptane, Combust. Flame 154 (2008) 153–163.
- [55] T. Lu, C.K. Law, Systematic approach to obtain analytic solutions of quasi steady state species in reduced mechanisms, J. Phys. Chem. A 110 (2006) 13202–13208.